



TECHNISCHE
UNIVERSITÄT
WIEN

Vienna University of Technology

DIPLOMARBEIT

Shape and local order in dendritic systems

ausgeführt am Insitut für

Theoretische Physik

der

Technischen Universität Wien

unter der Anleitung von

Ao. Univ. Prof. Dipl.-Ing. Dr. Gerhard Kahl

durch

Benedikt Pesendorfer, BSc

Hammer-Purgstall-Gasse 5/6

1020 Wien

Wien, Dezember 2014

(Benedikt Pesendorfer)

Zusammenfassung

Dendrimere sind verformbare polymerische Moleküle mit einer baumartigen inneren Struktur und gehören zu jener Klasse von Kolloidteilchen, die sich selbst zu supramolekularen Strukturen organisieren. Aufgrund ihrer relativ offenen inneren Struktur kann es bei der Wechselwirkung dieser Makromoleküle zu einem großen Volumenüberlapp kommen. Bei Dendrimerensystemen relativ hoher Dichte können Konfigurationen benachbarter Teilchen auftreten, die einer antinematischen Anordnung entsprechen. Dies kann als ein Indikator für eine zugrundeliegende A15 Struktur interpretiert werden. In der vorliegenden Arbeit werden die geometrische Form sowie die relative Orientierung einzelner Makromoleküle in dichten Systemen von Dendrimeren mit Hilfe von Molekulardynamik Simulationen untersucht. Ausgangspunkt ist die Beschreibung amphiphiler Dendrimere auf monomereischem Niveau. Mit Hilfe der Eigenwerte und Eigenvektoren des Gyrationstensors der Moleküle wird die geometrische Form und relative Orientierung der Teilchen charakterisiert. Aus diesen Informationen wird auf die räumliche Anordnung der Makromoleküle bei unterschiedlichen Temperaturen und Packungsdichten sowie bei geringerer Amphiphilität zurückgeschlossen.

Abstract

Dendrimers are typical soft matter molecules with a well defined internal tree-like structure, that are characterized by their ability to form considerable particle overlaps in dense systems. In the bulk an antinematic local order has been identified which represents strong indications for the occurrence of an A15 lattice. In this thesis we focus on the characterization of amphiphilic dendrimers in the bulk liquid. We use monomer-resolved molecular dynamic simulations and analyse the shape and relative orientation of these particles via the eigenvalues and eigenvectors of the gyration tensor. With this tool we further examine the short-range spatial and orientational order of these amphiphilic dendrimers at a variety of temperatures and packing fractions. Finally the degree of amphiphilicity of the dendrimers is modified in order to understand the reasons for the preference of the antinematic phase.

Contents

1. Introduction	1
2. Statistical mechanics	3
2.1. Basic concepts	3
2.2. The canonical ensemble	4
3. Model	6
3.1. Dendrimers	6
3.1.1. Historical information	7
3.2. Dendrimer simulation model	8
3.2.1. Amphiphilic dendrimers	8
4. Molecular dynamics simulations	13
4.1. Equations of motion	13
4.2. Verlet and velocity-Verlet algorithm	14
4.3. Periodic boundary conditions	14
4.4. Nosé-Hoover thermostat	15
5. Data analysis	17
5.1. Radial distribution function	17
5.2. Shape and orientation analysis	18
5.2.1. Gyration tensor	18
5.2.2. Orientation analysis	20
5.3. Implementation	23
5.3.1. Radial distribution function	23
5.3.2. Orientational order parameter	23
5.3.3. Conditional probability	24
6. Results	25
6.1. Shape of D7-type dendrimers (G2 to G8)	26
6.2. Influence of the packing fraction and of the temperature	29
6.2.1. $\phi_m = 0.248$	29
6.2.2. $\phi_m = 0.153$	35
6.2.3. $\phi_m = 0.095$	41
6.3. Tuning amphiphilicity	47
7. Conclusions	53

Appendices	56
A. Interaction parameters	57
B. Random distribution of α-parameter	60
Bibliography	62

1. Introduction

In our everyday life we are surrounded by *soft matter* [1] ranging from naturally occurring systems (such as protein solutions, DNA molecules or blood) over food (like milk or ice cream) to different kinds of industrial goods (e.g. rubber, gels, foams, paints, cosmetics and pharmaceuticals). The rigidity of materials which are considered to be *soft* is, as the nomenclature suggests, smaller against mechanical deformation compared to atomic materials and, therefore, soft matter molecules exhibit large responses to external forces. The hardness of materials can for instance be quantified via the shear modulus G that describes the resistance to a mechanical deformation; it can be estimated by [2]

$$G \approx \frac{\varepsilon}{\sigma^3}, \quad (1.1)$$

where ε is the typical interaction energy between two particles that are separated by a distance σ . In hard matter systems the interaction energy is given by the covalent bond energy between the atoms, thus $\varepsilon \approx 10^{-18}$ J [3], with typical bond lengths $\sigma \approx 10^{-10}$ m [3]. This results in a shear modulus for hard matter systems of the order of $G \approx 10^{12}$ N/m². In contrast, the size of soft matter particles ranges from nano- to micrometers ($\sigma \approx 10^{-8} - 10^{-6}$ m) with interaction energies between those particles of around 10^{-20} J [3] (such as van der Waals interactions or hydrogen bonds) leading to $G \approx 10^{-2} - 10^4$ N/m² [4]. Thus, hard and soft matter materials have highly different values of G , meaning that soft materials are much easier deformable than their hard counterparts. Even thermal fluctuations can be responsible for structural changes in soft matter systems with their interaction energy ε being comparable to the thermal energy at room temperature $k_B T \approx 10^{-21}$ J.

The soft matter molecules of interest in this work are dendrimers, i.e. highly branched synthetic macromolecules with a well defined internal tree-like structure. They are typically synthesized through an iterative procedure; the single components, so called *monomers* are successively added in layers where each layer is called a *generation* [5].

The scientific interest in dendrimers increased rapidly since they were first synthesized in 1978 by Vögtle et al. [6], especially after the late 1980s when Tomalia et al. [7] indicated possible applications, such as drug carriers and many other. Since then, dendrimers have been studied thoroughly in experiments (e.g., in Ref. [8, 9]), in computer simulations (e.g., in Ref. [10–13]) and in theory (a detailed review can be found in Ref. [14]).

Dendrimers were found to have an elongated shape at low generations and nearly spherical shape at higher generations with a considerable amount of back-folding, where monomers of higher generation mix with the inner parts of the molecule [15, 16]. They readily crystallize in different lattices (e.g. A15 and σ -phases [17, 18]) that are untypical for classical colloids which usually form body- and face-centered cubic crystals. At large densities a high amount of interpenetration was observed [19] in these dendrimer liquid crystals

leading to the A15 cubic lattice as observed in experiments [18].

In addition, theoretical studies of soft parallel ellipsoids interacting via repulsive Gaussian potential showed that they form elongated lattices if they are forced into alignment, e.g., by stretching the body-centered cubic crystal along the [001], [110] or [111] directions [20, 21]. These findings imply that parallel alignment of dendrimers is incompatible with the cubic symmetry, consequently, their relative orientation pattern in the A15 lattice must be more complex [22]. Georgiou et al. [16, 22] also found indications for the occurrence of the A15 lattice and suggested that the elongated shape of dendrimers may be the reason for the stability of this lattice as shown by Li et al. [19].

In this thesis we focus on the characterization of different types of dendrimers in the bulk liquid in terms of shape and relative orientation. We use the monomer resolved model for amphiphilic dendrimers which was the subject of research of Mladek et al. [12, 13, 23, 24]. The amphiphilic character of these dendrimers is induced by different interaction parameters between the inner and outer most monomers. We use monomer-resolved molecular dynamic simulations [25] to generate configurations belonging to the canonical ensemble. Thus, we analyze the shape and relative orientation of the dendrimers in the bulk based on the eigenvalues and eigenvectors of the radius of gyration tensor [26]. The aim of this work is to further examine the short range structure of these amphiphilic dendrimers at a variety of different temperatures and packing fractions, as well as, for less amphiphilic dendrimers in order to understand the reasons for the preference of the A15 as already observed for dendritic polymers by Zeng et. al. [18]. We also include results for the shape of amphiphilic dendrimers in the bulk for different values of the generation number.

The thesis is organized as follows:

- **Chapter 2** gives a brief overview of the key ideas of statistical mechanics with a focus on the canonical ensemble.
- **Chapter 3** presents an overview of relevant historical work on dendrimers as well as the simulation models used to describe these macromolecules in terms of interaction potentials.
- **Chapter 4** provides the basic ideas of molecular dynamics simulations which we use to obtain information about the observed systems.
- **Chapter 5** summarizes the quantities that we used to analyze the shape and relative orientation of dendrimers.
- **Chapter 6** is the main part in this theses as it contains the results of the shape and relative orientation analysis of the observed dendrimer liquids. We present the dependence of the shape of dendrimers in a bulk liquid on the generation number. Then we proceed by analyzing the changes in shape and relative orientation of dendrimer liquids when changing temperature and packing fraction. Furthermore, we also examine these properties for dendrimers with different amphiphilic behavior.
- **Chapter 7** summarizes our findings and gives an outlook on future work.
- **Appendices A & B**

2. Statistical mechanics

In this chapter we recall basic ideas of *statistical mechanics* with a focus on the *canonical ensemble*. A comprehensive introduction to the subject can be found, e.g., in Ref. [27].

2.1. Basic concepts

The microscopic state of a system of N spherical particles at a certain time t is fully determined by a point in the $6N$ -dimensional *phase space* that represents the $3N$ coordinates $\mathbf{r}_1(t), \mathbf{r}_2(t), \dots, \mathbf{r}_N(t)$ and $3N$ momenta $\mathbf{p}_1(t), \mathbf{p}_2(t), \dots, \mathbf{p}_N(t)$ of the particles. The dynamics of the system are governed by the Hamilton function $\mathcal{H}(\mathbf{r}^N, \mathbf{p}^N)$ and the equations of motion [28]

$$\frac{\partial \mathcal{H}(\mathbf{r}^N, \mathbf{p}^N)}{\partial \mathbf{p}_i} = \dot{\mathbf{r}}_i, \quad i = 1, \dots, N \quad (2.1)$$

and

$$\frac{\partial \mathcal{H}(\mathbf{r}^N, \mathbf{p}^N)}{\partial \mathbf{r}_i} = -\dot{\mathbf{p}}_i, \quad i = 1, \dots, N \quad (2.2)$$

where the dot denotes a time derivative.

Since the number of particles of typical macroscopic systems is usually of the order of $N \sim 10^{23}$, it is not possible to determine the exact phase space trajectory of the system. However, the aim of statistical mechanics is not to properly solve the equations of motion for each particle but rather to provide a conceptual understanding of the macroscopic variables of the system, such as pressure or temperature. For this purpose, we introduce the concept of an *ensemble*, i.e., a large number of realizations of a system whose microscopic states differ from each other but correspond to the same macroscopic state. Using this concept, a macroscopic observable $A(\mathbf{r}^N, \mathbf{p}^N)$ can be obtained by averaging the values of $A(\mathbf{r}^N, \mathbf{p}^N)$ over all possible microscopic states of the ensemble, i.e., the *ensemble average*

$$\langle A \rangle_{\text{en}}^M = \frac{1}{M} \sum_{i=1}^M A_i, \quad (2.3)$$

where A_i is the value of $A(\mathbf{r}^N, \mathbf{p}^N)$ of realization i of the system in the ensemble and M is the number of realizations considered. Assuming that the time-evolving system will eventually visit all (or a huge number of) the microscopic states during a long enough

period of time t , we can also determine a *time average* given by

$$\langle A \rangle_{\text{time}}^t = \frac{1}{t} \int_0^t dt' A(t'), \quad (2.4)$$

where $A(t')$ is the value of observable $A(\mathbf{r}^N, \mathbf{p}^N)$ at time t' . Thus, a system is called ergodic if

$$\lim_{M \rightarrow \infty} \langle A \rangle_{\text{en}}^M = \lim_{t \rightarrow \infty} \langle A \rangle_{\text{time}}^t, \quad (2.5)$$

where, due to the flow of the system through phase space, the time average is the same as the ensemble average since after an infinite amount of time all possible realizations are visited.

2.2. The canonical ensemble

In this thesis we consider a system of identical particles with fixed particle number N inside a fixed volume V and in thermal equilibrium with an infinite large heat bath, so that the system will have a fixed temperature T . The *partition function* of the canonical ensemble in the classical limit is given by [27]

$$Z(N, V, T) = \frac{h^{-3N}}{N!} \iint e^{-\mathcal{H}(\mathbf{r}^N, \mathbf{p}^N)/k_B T} d\mathbf{r}^N d\mathbf{p}^N, \quad (2.6)$$

where $\mathcal{H}(\mathbf{r}^N, \mathbf{p}^N)$ is the Hamiltonian of the system, $\beta = 1/k_B T$ with k_B being the Boltzmann constant, h is the Planck constant and $N!$ is needed to properly account for the indistinguishability of the particles. The partition function is of great importance since it links statistical mechanics with thermodynamics via

$$F(N, V, T) = -k_B T \log Z(N, V, T), \quad (2.7)$$

where $F(N, V, T)$ is the *Helmholtz free energy* which is the appropriate *thermodynamic potential* for a system of fixed N , V and T .

Since the partition function and therefore the free energy contain essentially the entire information about the macroscopic thermodynamic properties of the system, we can obtain all other thermodynamic state functions from $F(N, V, T)$ via suitable differentiations. For example, the internal energy U , i.e., the expectation value of the Hamiltonian of the system is given by

$$U = \left(\frac{\partial \beta F}{\partial \beta} \right)_{V, N}. \quad (2.8)$$

Further, the pressure P of the system is given by

$$P = - \left(\frac{\partial F}{\partial V} \right)_{N, T} \quad (2.9)$$

and the chemical potential μ , which measures the change in the Helmholtz free energy due to the addition of one particle in the system, by

$$\mu = \left(\frac{\partial F}{\partial N} \right)_{V,T} . \quad (2.10)$$

3. Model

3.1. Dendrimers

A polymer is a macromolecule consisting of many branched and linked molecules [29], where the single components, so called *monomers*, are connected through covalent bonds. *Dendrimers*, a very specific type of these polymeric macromolecules, are characterized by a well defined, repetitively and highly branched internal structure. Their name is based on the Greek word *dendron* for tree and describes the typical tree-like topology of these molecules (see Fig. 3.1). Typically, dendrimers are synthesized through an iterative reactive procedure, where branched monomers are successively added in layers, so-called *generations*. The last generation monomers are called the *end-groups*. In the following, dendrimers consisting of n generations are referred to as G_n dendrimers.

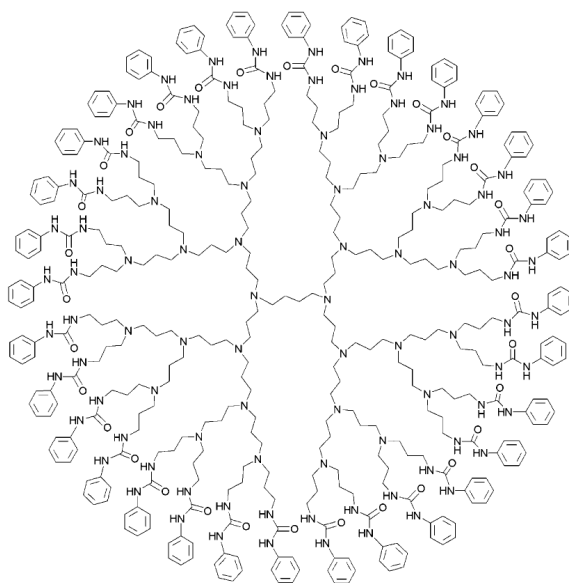


Figure 3.1.: Structure of a fourth-generation dendrimer. From: M. Ballauff and C. N. Likos [14]

In the case of regular dendrimers, this branching starts from a single central monomer of *functionality* f , which means that from there f polymer chains consisting of P bonds branch out, where P is the so-called *spacer length*. The central particle constitutes the zeroth generation. From the end of each chain again f chains with length P branch out, forming the next generation and so on. Thus, the three parameters functionality f (most commonly $f = 3$), spacer length P and the number of generations G characterize a single

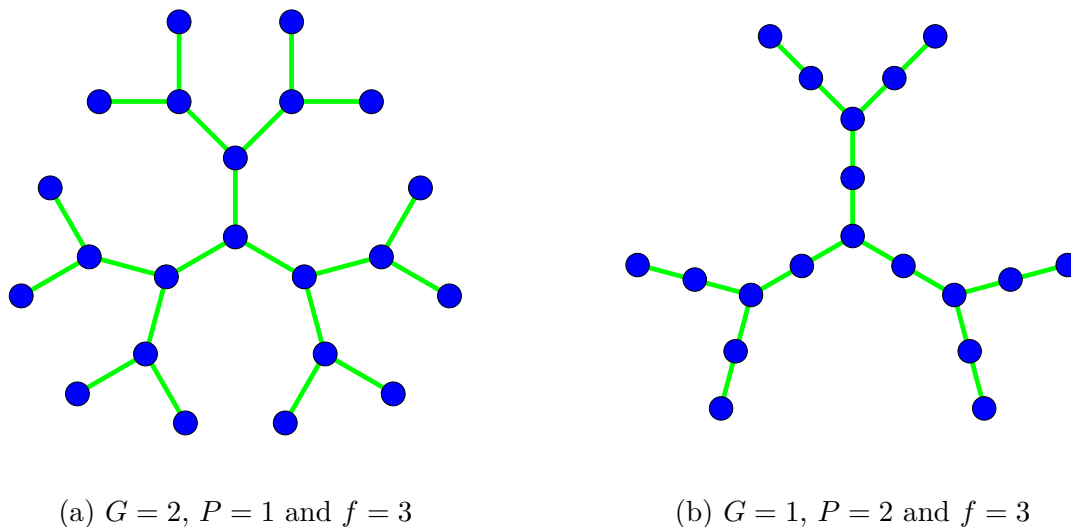


Figure 3.2.: Schematic representation of two dendrimers with given parameters. Branching starts from a single monomer. The monomers and bonds are colored in blue and green, respectively.

dendrimer (see Fig. 3.2). The total number of monomers N in a regular dendrimer is given by

$$N = 1 + fP \frac{(f-1)^{G+1} - 1}{f-2}. \quad (3.1)$$

The monomers corresponding to the last and outermost generation G form the *shell* of the dendrimer, while the rest forms the *core* of the dendrimer. The number of shell monomers N_s is given by

$$N_s = Pf(f-1)^G. \quad (3.2)$$

Nowadays, dendrimers are of relevance in a wide range of technological and medical applications, for example in the area of nanotechnology, as bio-sensors, as magnetic resonance image contrast agents or for gene transduction and drug delivery [30–37]. However, since their synthesis is rather time consuming and expensive, their commercial availability is limited to only a few substances [38].

3.1.1. Historical information

Ever since dendrimers were first synthesized in 1978 by Vögtle et al. [6] the scientific interest in those molecules increased rapidly. One reason for the numerous research activities carried out in this area was related to the question whether dendrimers show a so-called *dense-shell* or a *dense-core* conformation. In 1983 the dense-shell conformation was proposed in the theoretical work by Gennes et al. [39], where end-groups reside at the periphery of the macromolecule leaving a hollow core. However, in 1990 simulation studies by Lescanec and Muthukumar indicated [40] the contradicting dense-core model, where back-folding of the end monomers leads to end-groups mixing with the lower-generation

monomers in the inner part of the molecule. Initially, both the dense-shell and the dense-core predictions suffered from different short-comings, but it was the theoretical work performed by Boris and Rubinstein [41] that first supported the validity of the dense-core model, showing that the end-groups were distributed inside the body of the dendrimer and the monomeric density was proven to monotonically decay from the center of the molecule. These findings were in good agreement with computer simulations results [40, 42].

More recent investigations showed [43, 44], that the issue of dendrimer conformations can become even more complex, since certain dendrimers do not only exist in one of these two conformations but are also able to undergo a transition from the dense-core to the dense-shell conformation and vice versa, depending on the pH and/or the salt concentration of the solvent.

Fundamental for this thesis is a phenomenon occurring for certain types of dendrimers [12, 23], the formation of full molecular overlaps, so-called *clusters*. Likos et al. [45] established a criterion for cluster formation of molecules interacting via bounded, non-negative *effective potentials*, which arise as the intermolecular degrees of freedom are averaged out. They showed that clustering occurs when the Fourier transform of the effective interaction has negative components, these are so-called Q^\pm potentials.

3.2. Dendrimer simulation model

The architecture as well as the chemical nature of the monomers (such as size, softness and interactions) determine the behavior of a given dendrimer. In computer simulations the architecture of a dendrimer is described by the bonding interactions and the chemical nature of the monomers by their mutual interactions.

3.2.1. Amphiphilic dendrimers

In this work, we use the monomer resolved model for amphiphilic dendrimers introduced by Mladek et al. [23, 24], which is based on a previous model of Welch and Muthukumar [43]. It was shown that their effective interactions belong to the class of Q^\pm potentials [12] and thus they are suitable colloids for cluster formation [45]. Their spacer length is $P = 1$ while their functionality is $f = 3$. Here, dendrimers are considered where branching starts from a central bond rather than a central monomer. *Amphiphilic dendrimers* are built up by solvophobic core monomers, labeled by 'C', and solvophilic shell monomers, representing the outermost units, labeled by 'S'. The total number of monomers in a dendrimer of generation G is then given by

$$n(G) = 2(2^{G+1} - 1), \quad (3.3)$$

including $(2^{G+1} - 2)$ core monomers and 2^{G+1} shell monomers.

As a consequence of distinguishing between shell and core monomers, three different interaction types have to be defined, labeled as 'CC' for interactions between two core

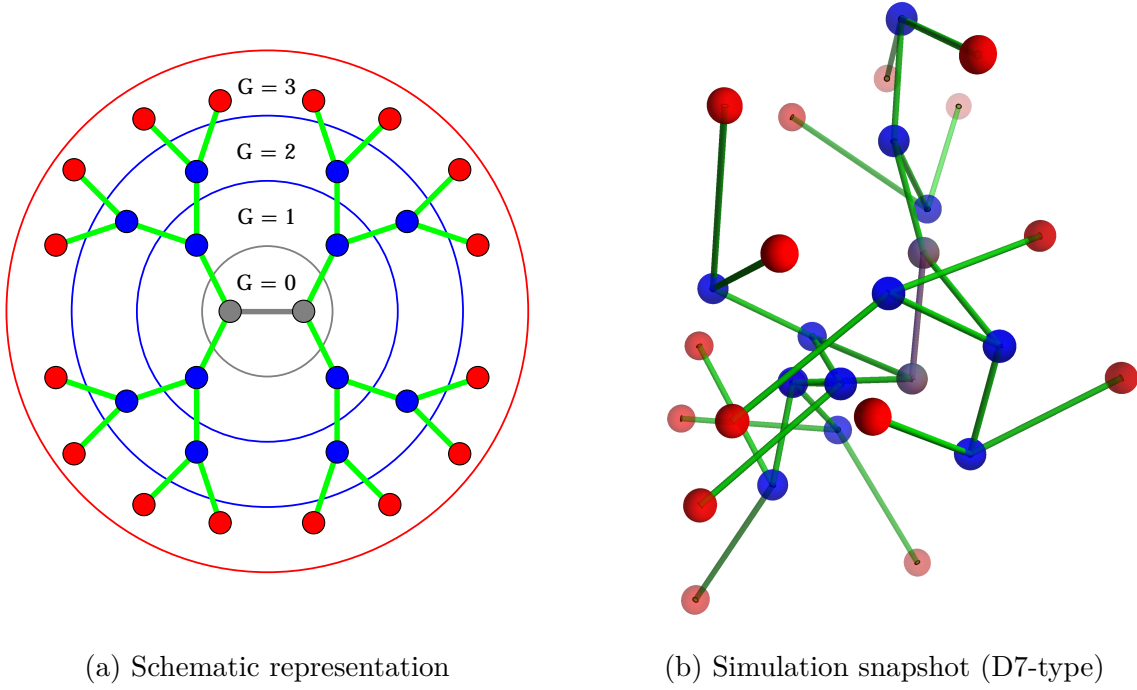


Figure 3.3.: Two representations of an amphiphilic G3 dendrimer, the core (C) and the shell (S) monomers are coloured in blue and red, respectively. The bonds are coloured in green. For better clarity, the two central monomers and the corresponding central bond are coloured grey.

monomers, 'CS' for interactions between core and shell monomers and 'SS' for interactions between two shell monomers. We denote the different types by the subscript $\mu\nu$.

Bonded monomers of the dendrimer interact via the *finitely extensible non-linear elastic (FENE) potential* [46]

$$\beta\Phi_{\mu\nu}^{\text{FENE}}(r) = -K_{\mu\nu} R_{\mu\nu}^2 \ln \left(1 - \left(\frac{r - l_{\mu\nu}^0}{R_{\mu\nu}} \right)^2 \right), \quad (3.4)$$

where $K_{\mu\nu}$ represents the elasticity of the bond, $R_{\mu\nu} = (l_{\mu\nu}^{\max} - l_{\mu\nu}^{\min})/2$ restricts the bond length to an interval $[l_{\mu\nu}^{\min}, l_{\mu\nu}^{\max}]$ and $l_{\mu\nu}^0 = (l_{\mu\nu}^{\min} + l_{\mu\nu}^{\max})/2$ is the equilibrium bond-length. In addition, all monomers separated by a distance r interact via the Morse potential [47]

$$\beta\Phi_{\mu\nu}^{\text{Morse}}(r) = \varepsilon_{\mu\nu} \{ [\exp(-\alpha_{\mu\nu}(r - d_{\mu\nu})) - 1]^2 - 1 \}, \quad (3.5)$$

where $\varepsilon_{\mu\nu}$ accounts for the strength of the interaction, $d_{\mu\nu}$ represents the radius of the monomer and $\alpha_{\mu\nu}$ tunes the attraction.

We focus on the family of dendrimers referred to as D7 [12]. The corresponding parameters are shown in Table 3.1. For all interaction parameters throughout this thesis we use the diameter of the core monomers of the D7-type, labeled $d_{\text{CC}}^{\text{D7}}$, as the unit of length. We use a general cut-off distance $r_c = 2.8 d_{\text{CC}}^{\text{D7}}$ for all Morse interactions.

D7 ($x = 1.00$)

FENE	$K_{\mu\nu}(d_{CC}^{D7})^2$	$l_{\mu\nu}^0/d_{CC}^{D7}$	$R_{\mu\nu}/d_{CC}^{D7}$
CC	40	1.8750	0.3750
CS	20	2.8125	0.5625
Morse	$\varepsilon_{\mu\nu}$	$\alpha_{\mu\nu}d_{CC}^{D7}$	$d_{\mu\nu}/d_{CC}^{D7}$
CC	0.714	6.4	1.00
CS	0.014	19.2	1.25
SS	0.014	19.2	1.50

Table 3.1.: Interaction parameters of the potentials Eq.(3.4) and Eq.(3.5) for D7-type dendrimers.

In addition, we also use certain variants of the original D7-type dendrimer to tune the amphiphilicity of a given molecule. To this end, we use a parameter $x \in [0, 1]$ which linearly modifies the CC FENE parameters to those corresponding to CS as well as the CC and CS Morse parameters to those of SS. Thus, D7 (i.e. $x = 1.00$) will be the most amphiphilic dendrimer, while for $x = 0.00$ the difference between shell and core monomers vanishes completely (the corresponding interaction parameters are shown in Table 3.2). We introduce six new types of dendrimers called X1 ($x = 0.00$), X2 ($x = 0.25$), X3 ($x = 0.50$), X4 ($x = 0.75$), X5 ($x = 0.90$) and X6 ($x = 0.95$) in order of increasing amphiphilicity. Thus, X2, X3, X4, X5 and X6 represent just “interpolations” between the D7 and X1 dendrimers. Their corresponding interaction parameters are presented in Appendix A.

X1 ($x = 0.00$)

FENE	$K_{\mu\nu}(d_{CC}^{D7})^2$	$l_{\mu\nu}^0/d_{CC}^{D7}$	$R_{\mu\nu}/d_{CC}^{D7}$
CC	20	2.8125	0.5625
CS	20	2.8125	0.5625
Morse	$\varepsilon_{\mu\nu}$	$\alpha_{\mu\nu}d_{CC}^{D7}$	$d_{\mu\nu}/d_{CC}^{D7}$
CC	0.014	19.2	1.50
CS	0.014	19.2	1.50
SS	0.014	19.2	1.50

Table 3.2.: Interaction parameters of the potentials Eq. (3.4) and Eq. (3.5) for X1-type dendrimers.

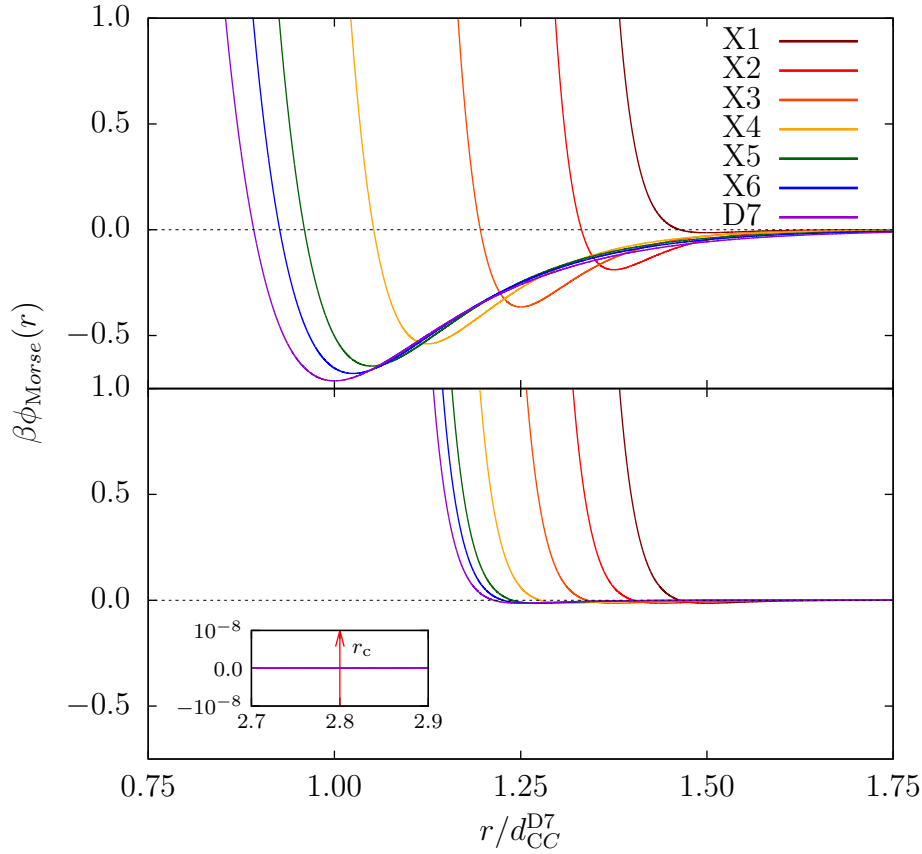


Figure 3.4.: Illustration of the Morse interaction potentials (see Eq. (3.5)) for the different types of dendrimers used in this thesis (i.e., X1 to X6 and D7). The top panel shows the respective CC potentials and the lower panel the respective CS potentials. The parameters of the respective SS potentials are the same for all types of dendrimer and are set equal to the parameters of the CC/CS interaction of X1. The inset shows a close-up at the cutoff radius $r_c = 2.8 d_{\text{CC}}^{\text{D7}}$ that is used for all Morse interactions; the cut-off radius is represented by a red arrow.

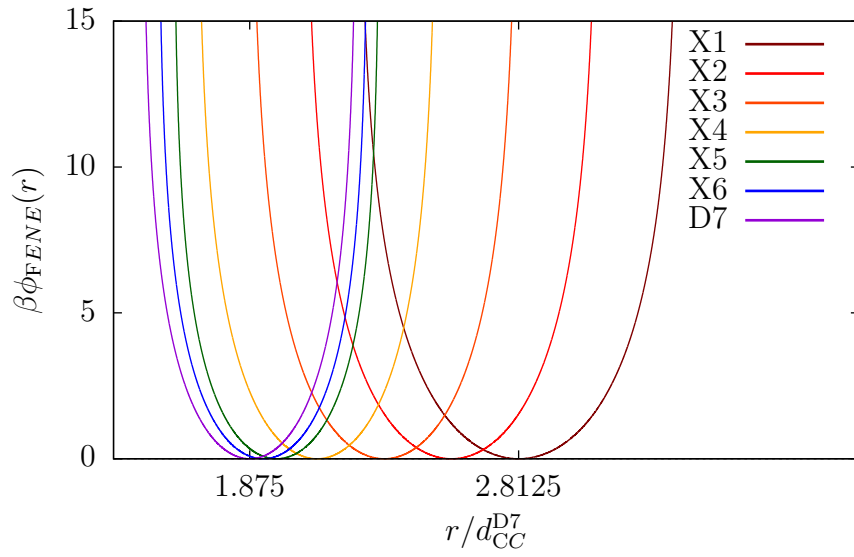


Figure 3.5.: Illustration of the CC FENE interaction potentials (see Eq. (3.4)) for the different types of dendrimers used in this thesis (i.e., X1 to X6 and D7). The parameters of the respective CS potentials are the same for all types of dendrimer and are equal to the parameters of the CC interaction of X1.

4. Molecular dynamics simulations

Molecular dynamics (MD) *simulation* is a simulation technique for computing the trajectories of particles in terms of particle positions and velocities in a many-body system by numerically solving Newton's equations of motion. It is a widely used method to obtain numerical results for problems with a huge number of degrees of freedom that cannot be solved analytically. Moreover and in contrast to Monte Carlo [48] simulations, it provides a numerical approximation for the trajectories of all particles in the observed system.

4.1. Equations of motion

The observed system consists of N particles interacting via a potential $U(\mathbf{r}^N)$, where \mathbf{r}^N is a N -dimensional vector and its i -th component represents the position of particle i . Then, the velocity \mathbf{v}_i of particle i with mass m_i is given by the time derivative $\dot{\mathbf{r}}_i = \frac{d}{dt}\mathbf{r}_i$. The dynamics of the system are described by the Lagrangian [28]

$$\mathcal{L} = \sum_{i=1}^N \frac{m_i}{2} \dot{\mathbf{r}}_i^2 - U(\mathbf{r}^N). \quad (4.1)$$

We can now use the Lagrangian equations of motion

$$\frac{d}{dt} \left(\frac{\partial \mathcal{L}}{\partial \dot{\mathbf{r}}_i} - \frac{\partial \mathcal{L}}{\partial \mathbf{r}_i} \right) = 0, \quad i = 1, \dots, N \quad (4.2)$$

to obtain $3N$ coupled second-order differential equations

$$m_i \ddot{\mathbf{r}}_i = \mathbf{f}_i, \quad i = 1, \dots, N \quad (4.3)$$

with $\ddot{\mathbf{r}}_i = \frac{d^2}{dt^2}\mathbf{r}_i$ being the acceleration of particle i resulting from the force exerted on this particle by all the other particles via $U(\mathbf{r}^N)$

$$\mathbf{f}_i = -\nabla_{\mathbf{r}_i} U(\mathbf{r}^N), \quad i = 1, \dots, N. \quad (4.4)$$

In this thesis we use MD simulations to obtain the time evolution of the system after starting from initial positions and velocities until the system has *equilibrated*. The system is considered to be equilibrated once the regarded parameters (e.g., the potential energy $U(\mathbf{r}^N)$ of the system) stop drifting and fluctuate around a constant value.

4.2. Verlet and velocity-Verlet algorithm

The *Verlet algorithm* [49] is a commonly used method in MD simulations for numerically integrating the equations of motion. With position $\mathbf{r}_i(t)$ and force $\mathbf{f}_i(t)$ corresponding to particle i at time t and the position a time increment δt earlier $\mathbf{r}_i(t - \delta t)$ at time $t - \delta t$ we can determine the particle's position at the following time step $t + \delta t$

$$\mathbf{r}_i(t + \delta t) = 2\mathbf{r}_i(t) - \mathbf{r}_i(t - \delta t) + \frac{\mathbf{f}_i(t)}{m_i} \delta t^2. \quad (4.5)$$

This expression can be easily obtained by adding two second-order Taylor expansions about $\mathbf{r}_i(t)$ one evaluated at $t + \delta t$ and the other at $t - \delta t$

$$\begin{aligned} \mathbf{r}_i(t + \delta t) &= \mathbf{r}_i(t) + \mathbf{v}_i(t)\delta t + \frac{\mathbf{f}_i(t)}{2m_i} \delta t^2, \\ \mathbf{r}_i(t - \delta t) &= \mathbf{r}_i(t) - \mathbf{v}_i(t)\delta t + \frac{\mathbf{f}_i(t)}{2m_i} \delta t^2. \end{aligned} \quad (4.6)$$

Thus, the velocities \mathbf{v}_i are not appearing in (4.5) and are therefore not needed in the Verlet algorithm.

The integration scheme used throughout this work is a modification to the above described basic Verlet algorithm and is known as the *velocity-Verlet algorithm* [50] which includes the velocities in the calculation and offers enhanced precision. Positions \mathbf{r}_i and velocities \mathbf{v}_i are obtained via the Taylor expansions

$$\begin{aligned} \mathbf{r}_i(t + \delta t) &= \mathbf{r}_i(t) + \mathbf{v}_i(t)\delta t + \frac{\mathbf{f}_i(t)}{2m_i} \delta t^2, \\ \mathbf{v}_i(t + \delta t) &= \mathbf{v}_i(t) + \frac{1}{2m_i} [\mathbf{f}_i(t) + \mathbf{f}_i(t + \delta t)] \delta t. \end{aligned} \quad (4.7)$$

4.3. Periodic boundary conditions

Above all, the size of the system that is to be simulated is limited by the time needed for execution of the program on today's computers, typically CPU-days to CPU-years are needed. Hence, only a small, compared to system sizes in reality, number of particles $N \ll 10^{23}$ can be handled in a feasible amount of time. To obtain the properties of a macroscopic sample via molecular simulations *periodic boundary conditions* [51] are applied where the finite simulation box is treated as the primitive cell of an infinite periodic lattice of identical cells (see Fig. 4.1). As a consequence, no walls are present at the boundaries of the original cell. When a particle moves inside its original cell, all its periodic images in the neighboring cells move in exactly the same way. In case a particle passes the boundary of the cell, it reappears on the opposite side moving in the same direction with the same velocity. Therefore, the number of particles in the simulation cell is conserved. Under these conditions, particle i would then interact not only with all other particles in the same cell but also with all the other particles, including its own periodic

images in all the other cells. This would thus lead to a sum with an infinite number of terms when calculating the potential energy and the resulting force. However, for interactions of short-range, where interactions with neighboring particles that are closer than some cutoff distance r_c are dominating, we restrict this summation by making an approximation. For a cutoff distance smaller than half of the box length $r_c \leq L/2$ only interactions of a given particle with the nearest periodic image of (at most) all other particles are considered. This is referred to as the *minimum image convention* [25].

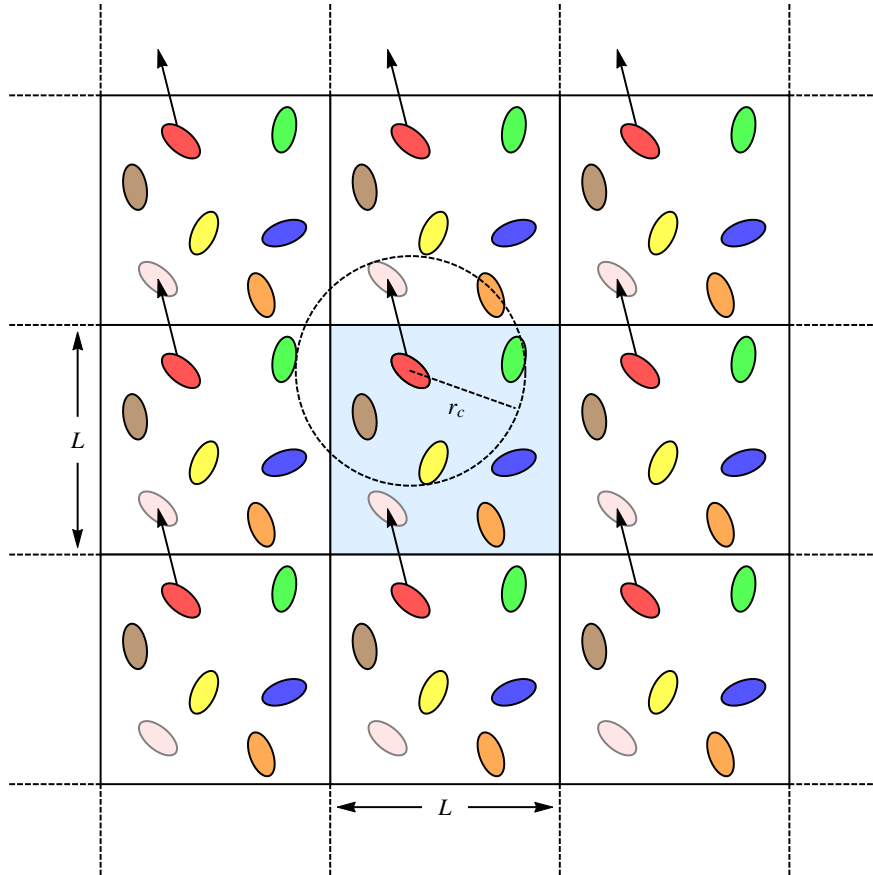


Figure 4.1.: A two-dimensional system (at the center and colored in blue) with box length L and its periodic images as used when applying periodic boundary conditions. Particles can enter and leave each box across each of the four edges. The cutoff radius r_c is shown. Idea from Ref. [25]

4.4. Nosé-Hoover thermostat

In order to simulate a canonical ensemble (NVT) with a constant number of particles N , constant volume V and constant temperature T in molecular dynamics simulations Nosé [52] proposed an extended Lagrangian with an additional degree of freedom s that

represents the heat bath

$$\mathcal{L} = \sum_{i=1}^N \frac{m_i}{2} \dot{\mathbf{r}}_i^2 - U(\mathbf{r}^N) + \frac{Q}{2} \dot{s}^2 - (N_f + 1) k_B T \ln s, \quad (4.8)$$

where $N_f = 3N$ is the number of degrees of freedom, k_B is the Boltzmann constant, T is the specified temperature and Q is a virtual mass of the heat bath, which controls the rate of temperature fluctuations. The Nosé-Hoover thermostat, with the heat bath being an integral part of the system, defines a deterministic integration method which keeps the temperature around a desired value.

5. Data analysis

This chapter summarizes the post-processing methods that we used for analyzing the data output (i.e., center-of-mass and radius of gyration tensor of all dendrimers) obtained from our MD simulations.

5.1. Radial distribution function

For spatially homogeneous and isotropic systems the *radial distribution function* for a canonical ensemble with N particles in a volume V at temperature T can be written as [25]

$$g(r) = \frac{V}{N^2} \left\langle \sum_{i=1}^N \sum_{\substack{j=1 \\ j \neq i}}^N \delta(\mathbf{r} - \mathbf{r}_{ij}) \right\rangle, \quad (5.1)$$

where $\delta(\mathbf{r})$ is the Dirac delta function and \mathbf{r}_{ij} denotes the vector between the positions of particles i and j . $g(r)$ is related to the probability of finding a pair of particles separated by a distance r relative to the probability expected for a random spatial distribution of the particles at the same density.

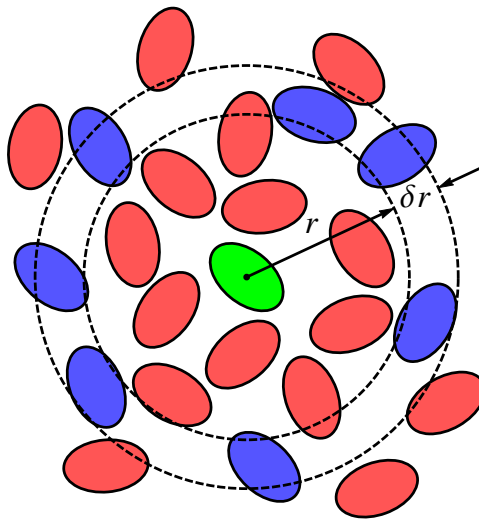


Figure 5.1.: Schematic representation of the calculation of $g(r)$ in two dimensions. The blue particles are considered in the calculation of $g(r)$ at distances r to $r + \delta r$ from the green, central particle.

5.2. Shape and orientation analysis

To obtain information about the shape and relative orientation of the molecules, we analyze their relative positions and characterize each molecule in terms of shape and orientation using their corresponding monomer positions.

5.2.1. Gyration tensor

The *gyration tensor* \mathcal{S} is a commonly used measure for the shape of polymers [53, 54] and is directly related to the moment of inertia tensor $\mathcal{I} = \text{Tr}(\mathcal{S}) \text{diag}(1, 1, 1) - \mathcal{S}$. [54] For a number of N particles at positions $\mathbf{r}_i = (x_i, y_i, z_i)$ with their corresponding center-of-mass at position $\mathbf{R}_{\text{cm}} = (x_{\text{cm}}, y_{\text{cm}}, z_{\text{cm}})$ the gyration tensor is defined as

$$\mathcal{S}_{\tau\tau'} = \frac{1}{N} \sum_{i=1}^N (\tau_i - \tau_{\text{cm}})(\tau'_i - \tau'_{\text{cm}}), \quad (5.2)$$

where $\tau, \tau' = x, y, z$.

The trace of \mathcal{S} is the square of a fundamental quantity, i.e., the *radius of gyration* R_g which characterizes the size of macromolecules

$$R_g^2 = \text{Tr}(\mathcal{S}) = \frac{1}{N} \sum_{i=1}^N (\mathbf{r}_i - \mathbf{R}_{\text{cm}})^2. \quad (5.3)$$

R_g is a rough measure of the overall size of a macromolecule (see Fig. 5.2). However, more detailed information about the shape of the molecule can be obtained from the gyration tensor when considering its corresponding eigensystem.

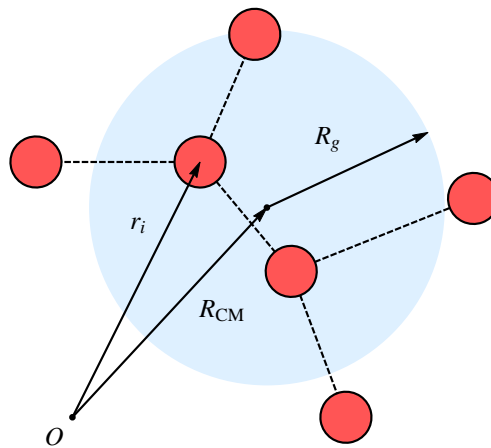


Figure 5.2.: Schematic two-dimensional representation of the radius of gyration R_g for a molecule which here consists of six particles at positions r_i colored in red. The blue sphere has a radius of R_g and its center is positioned at the center-of-mass of the molecule R_{cm} .

Eigenvalues and eigenvectors

Since \mathcal{S} is a real, symmetric 3×3 matrix it can be transformed into a diagonal matrix

$$\mathcal{S}_{\text{diag}} = \mathcal{P}\mathcal{S}\mathcal{P}^T = \begin{bmatrix} E_1 & 0 & 0 \\ 0 & E_2 & 0 \\ 0 & 0 & E_3 \end{bmatrix}, \quad (5.4)$$

where \mathcal{P} is a suitable transformation matrix, \mathcal{P}^T is its transpose and E_1, E_2, E_3 are the three eigenvalues of \mathcal{S} in descending order ($E_1 \geq E_2 \geq E_3$). The corresponding normalized eigenvectors are $\hat{\mathbf{e}}_1, \hat{\mathbf{e}}_2$ and $\hat{\mathbf{e}}_3$.

Shape analysis

Since the trace of \mathcal{S} is an invariant under the transformation (5.4) it follows with the definition of the radius of gyration (5.3) that

$$R_g^2 = \text{Tr}(\mathcal{S}) = E_1 + E_2 + E_3. \quad (5.5)$$

The radius of gyration describes the shape of the macromolecule as a *sphere* with radius R_g and its center located at the center-of-mass of the molecule (see Fig. 5.3a). However, if the macromolecule is not spherically symmetric a spherical shape is not a good representation. Measures for a deviation from spherical symmetry can be gained by comparing the traceless form of \mathcal{S} [53]

$$\hat{\mathcal{S}} = \mathcal{S} - \frac{1}{3}\text{Tr}(\mathcal{S}) \text{diag}(1, 1, 1) \quad (5.6)$$

with an another traceless tensor defined as [55]

$$\hat{\mathcal{S}} = b \text{diag}(2/3, -1/3, -1/3) + c \text{diag}(0, 1/2, -1/2). \quad (5.7)$$

By comparing (5.6) with (5.7) we can identify the *asphericity* (b) and the *acylindricity* (c) as

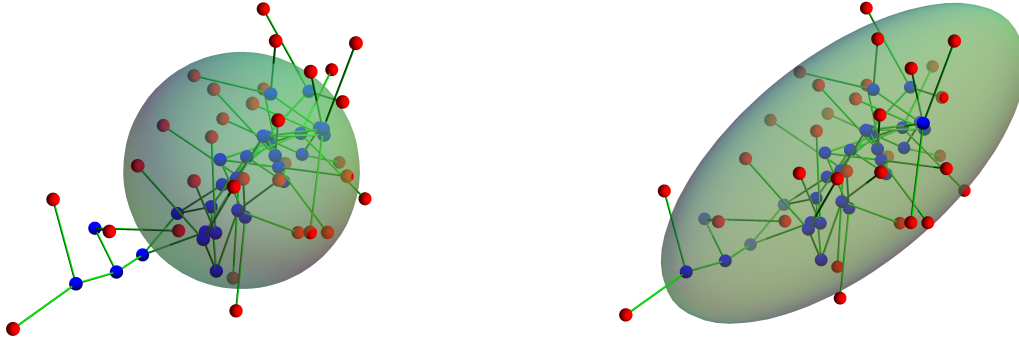
$$b = E_1 - \frac{1}{2}(E_2 + E_3), \quad b \geq 0 \quad (5.8)$$

$$c = E_2 - E_3, \quad c \geq 0. \quad (5.9)$$

A value $b = 0$ can correspond either to a spherical, tetrahedral or higher symmetry of the molecule. If the shape of the molecule is cylindrically symmetric, then $c = 0$.

Another parameter to characterize the asphericity, called the *relative shape anisotropy*, as defined in Ref. [26], is given by

$$\delta = 1 - 3 \frac{E_1 E_2 + E_1 E_3 + E_2 E_3}{(E_1 + E_2 + E_3)^2}, \quad 0 \leq \delta \leq 1. \quad (5.10)$$



(a) The shape is described by a sphere with its center located at the center of mass and radius R_g .

(b) The shape is described by an ellipsoid with its center located at the center-of-mass and semi-axes $\sqrt{3E_1}$, $\sqrt{3E_2}$ and $\sqrt{3E_3}$.

Figure 5.3.: Two possibilities to approximate the shape of a macromolecule. As an example a dendrimer of fourth generation with its 62 atoms and 61 bonds is shown. The core atoms are colored blue, the shell atoms red and the bonds green. The parameters for the shown dendrimer are: $R_g = 3.55$, $b = 4.02$, $c = 1.53$, $\delta = 0.11$, $E_1 = 6.87$, $E_2 = 3.62$ and $E_3 = 2.09$.

Its value ranges from $\delta = 0$ when the structure has spherical symmetry to $\delta = 1$ when the structure is of linear shape.

Furthermore, the eigenvalues of \mathcal{S} can be used to approximate the shape of the macromolecule by an *ellipsoid*. Then the square roots of three times the eigenvalue (i.e., $\sqrt{3E_1}$, $\sqrt{3E_2}$ and $\sqrt{3E_3}$) represent the mutually orthogonal semi-axes of the ellipsoid with its center being located at the center-of-mass (see Fig. 5.3b) [54].

5.2.2. Orientation analysis

For a macromolecule with no spherical symmetry (i.e., not all eigenvalues of \mathcal{S} are the same) corresponding eigenvectors can be used to assign an orientation to the molecule by interpreting $\hat{\mathbf{e}}_1$, $\hat{\mathbf{e}}_2$ and $\hat{\mathbf{e}}_3$ as the direction of its maximum, medium and minimum extension, respectively. With this information the relative orientation of two macromolecules that are a center-to-center distance r apart from each other can be quantified by *orientational correlation functions* [56, 57]. The most commonly used orientational correlation function is based on the second order Legendre polynomial [58] and is referred to as the *Herman's orientation function* [59–61]

$$S = \frac{1}{2} [3 (\cos \theta)^2 - 1], \quad (5.11)$$

where θ is the relative angle between the eigenvectors $\hat{\mathbf{e}}_{1,i}$ and $\hat{\mathbf{e}}_{1,j}$ of the macromolecules i and j with $\cos \theta = \hat{\mathbf{e}}_{1,i} \cdot \hat{\mathbf{e}}_{1,j}$ (see Fig. 5.4).

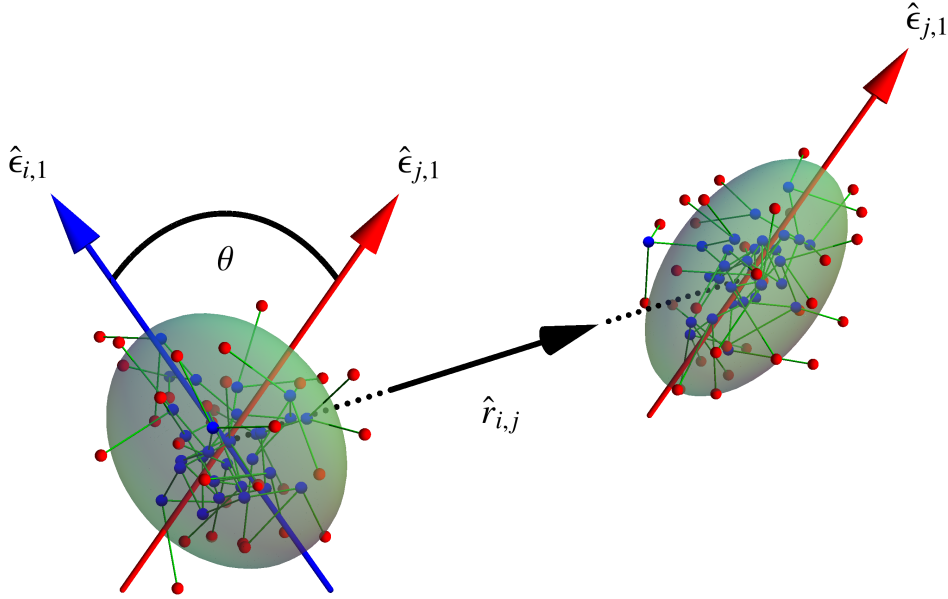


Figure 5.4.: Schematic representation of the parameters used for analyzing the respective orientation of two molecules which are here represented by two dendrimers of fourth generation as described in Fig. 5.3b. The angle θ between the unit eigenvectors of the long axes $\hat{\epsilon}_{1,i}$ and $\hat{\epsilon}_{1,j}$ is given by $\cos \theta = \hat{\epsilon}_{1,i} \cdot \hat{\epsilon}_{1,j}$. $\hat{r}_{i,j}$ is the unit center-to-center vector between the molecules i and j . The orientation parameters for the shown dendrimers are: $\theta = 70^\circ$, $S = -0.32$ and $\alpha = 0.11$. The lengths of the unit vectors $\hat{\epsilon}_{1,i}$, $\hat{\epsilon}_{1,j}$ and $\hat{r}_{i,j}$, shown in the plot, are not drawn to scale for convenience. Idea from Ref. [16]

For perfectly aligned molecules (i.e., $\hat{\epsilon}_{1,i}$ and $\hat{\epsilon}_{1,j}$ are parallel) the orientation function is $S = 1$, whereas for molecules that are perpendicular $S = -1/2$, when averaging over randomly oriented molecules $S = 0$.

Since S only characterizes the angle between the axes of maximum extension $\hat{\epsilon}_1$ of two molecules and does not take into account their relative position to each other, we introduce another parameter to classify the relative configuration of two molecules

$$\alpha = \frac{1}{2} \left[(\hat{\epsilon}_{1,i} \cdot \hat{r}_{i,j})^2 + (\hat{\epsilon}_{1,j} \cdot \hat{r}_{i,j})^2 \right], \quad (5.12)$$

where $\hat{r}_{i,j}$ is the unit vector pointing from the center-of-mass of molecule i to the center of mass of molecule j (see Fig. 5.4). Table 5.1 presents six basic configurations of two macromolecules and their corresponding values of α and S .

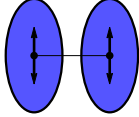
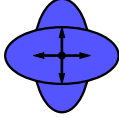
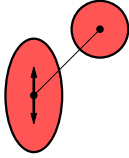
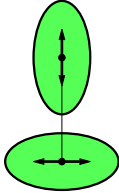
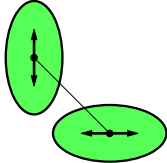
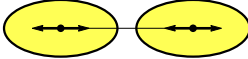
schematic	α	S	symbol
	0	1	
	0	-0.5	+
	0.25	-0.5	I[•]
	0.5	-0.5	⊥
	0.5	-0.5	L
	1	1	--

Table 5.1.: Characteristic configurations each shown with a schematic representation and with their values of α and S and a corresponding symbol. Copied from Ref. [16]

5.3. Implementation

This section provides further information of how the presented parameters are being used in describing the data output of our molecular simulations and how they are computed. Since we are mainly interested in the relative orientation of two dendrimers separated by a center-of-mass distance r , we use r and the parameter α from Eq. (5.12) to build two-dimensional expressions for the pair distribution function $g(r)$ presented in section 5.1, for the orientational correlation function S as described in section 5.2.2 and also for the conditional probability.

5.3.1. Radial distribution function

From Eq. (5.1) we can formulate an algorithm for the calculation of $g(r)$ for N particles within a cubic box of side length L [62, 63]:

- (i) Therefore, we divide the r -space in N_r^{bin} number of bins and initialize an array with N_r^{bin} elements which are all set to 0. The spatial step is set to $\Delta r = L/2N_r^{\text{bin}}$ in order to cover the range $[0, L/2]$.
- (ii) The number of pairs n_i^{pair} whose distance is within $i\Delta r \leq r < (i+1)\Delta r$ is counted (note that each pair is counted twice because of Eq. (5.1), e.g. 1-2 and 2-1) and written in the corresponding bin for every i with the bin number $i \in [0, N_r^{\text{bin}} - 1]$
- (iii) Then assuming that Δr is sufficiently small we can approximate Eq. (5.1) by

$$g(r_i + 0.5\Delta r) = \frac{V n_i^{\text{pair}}}{N^2 \Delta V_i}, \quad (5.13)$$

where $\Delta V_i = \frac{4}{3}\pi(r_{i+1}^3 - r_i^3)$ and $r_i = i\Delta r$.

Note that the calculation is restricted within a distance equal to $L/2$, which is the radius of the largest sphere that can be inscribed in a cube of side length L .

In order to get the two-dimensional radial distribution function $g(r, \alpha)$ [16], we also divide the orientational parameter α -space ($\alpha \in [0, 1]$) in N_α^{bin} equally sized bins. This way we get one one-dimensional histogram of α for each value of r and therefore $N_r^{\text{bin}} N_\alpha^{\text{bin}}$ pairs of (r_i, α_j) with $i \in [0, N_r^{\text{bin}} - 1]$ and $j \in [0, N_\alpha^{\text{bin}} - 1]$. After counting the number of pairs for each bin (r, α) we first normalize the histogram as before in Eq. (5.13) and additionally according to the random distribution of the α parameter (see Appendix B or Ref. [16]).

5.3.2. Orientational order parameter

The orientational order parameter $S(r, \alpha)$ [16] is a function that describes the value of S (5.2.2) for two molecules with parameter α that are a center-to-center distance r away from each other. The calculation is performed in exactly the same way as for $g(r, \alpha)$ (see Section 5.3.1) with the only difference of not counting pairs but calculating the mean

value of S for each bin (r, α) . The histogram is then normalized according to the random distribution of the α parameter (see Appendix B or Ref. [16]).

5.3.3. Conditional probability

The conditional probability $P(r, \alpha)$ [16] describes the probability of finding a pair of molecules with parameter α if they are a distance r apart from each other. Again, the calculation is done in the same way as for $g(r, \alpha)$ (see Section 5.3.1) with the difference that normalization is done by dividing the number of pairs in each bin (r_i, α_j) with the total number of counted pairs at the corresponding distance r_i . The histogram is then normalized according to the random distribution of the α parameter (see Appendix B or Ref. [16]).

6. Results

In this chapter we summarize the results obtained in a bulk liquid for different generation numbers (Sec. 6.1), at a variety of different temperatures and packing fractions (Sec. 6.2) and for the different types of dendrimers (Sec. 6.3) as introduced in Sec. 3.2.1. We start by analyzing the shape of D7-type dendrimers of different generations (G2 to G8) in a bulk liquid. Then we focus on G4 dendrimers and we investigate the positional and orientational properties of dendrimers in a bulk liquid of G4 D7-type dendrimers at different temperatures and different packing fractions. Furthermore, we analyze G4 dendrimers with different types of interaction parameters, i.e., X1-type to X6-type dendrimers.

To obtain the relevant information, we perform NVT MD simulations using the LAMMPS simulation package [64] with the implemented Nosé-Hoover thermostat (see chapter 4).

For all simulations we use a time step $\Delta t = 5 \cdot 10^{-4} d_{CC}^{D7} \sqrt{m/\varepsilon_{CC}^{D7}}$, whit the mass of the monomers m set to unity. Furthermore, we use a damping factor $T_{\text{damp}} = 1000 \Delta t$ defined as $Q = (N_f + 1)\beta T_{\text{damp}}^2$ with Q being the virtual mass and N_f the number of degrees of freedom of the system (introduced in subsection 4.4).

The packing fraction of the monomers ϕ_m , defined in Ref. [65], is used as a measure of the density for the liquid phase

$$\phi_m = \frac{N_D}{V_{\text{system}}} \frac{\pi}{6} \left(N_{\text{core}} (d_{CC}^{D7})^3 + N_{\text{shell}} (d_{SS}^{D7})^3 \right), \quad (6.1)$$

where N_{core} and N_{shell} denote the number of core and shell monomers and $d_{CC}^{D7} = 1.5 d_{SS}^{D7}$. $V_{\text{system}} = L^3$ is the volume of the system with L being the length of the cubic simulation box. Throughout, we consider in the simulations an ensemble consisting of $N_D = 220$ dendrimers, representing a compromise between accuracy and computational effort [16, 22].

To create the initial configurations we use an algorithm which generates the desired number of dendrimers N_D within a cubic box of defined length: the algorithm starts with one isolated dendrimer and places all monomers with respect to their restrictions due to bonding and excluded volume interaction. This is achieved by randomly chosen positions, where positions that lie within or without a certain distance interval to other monomers are rejected. The procedure is repeated until all N_D dendrimers and thus their respective monomers are placed within the cubic simulation box.

However, it is essentially impossible to achieve a dense packing with the described algorithm due to overlaps of the monomers. We therefore start from a larger simulation box and use the `fix deform`¹ command in LAMMPS which reduces the box length linearly at every time step and rescales the positions of all particles accordingly until the desired

¹http://lammps.sandia.gov/doc/fix_deform.html (online 11.12.2014)

box length is reached.

This algorithm performs in a satisfying way for generation numbers up to G5, however, for higher generation numbers we have to start from an initial single dendrimer due to the fact that the algorithm is not able to appropriately place multiple dendrimers in even huge simulation boxes. Thus, we reproduce this single dendrimer box N_D -times by using the command `replicate`² in LAMMPS, which replicates a given simulation box and places the resulting box next to the original one; thereby all properties of the initial particles, such as bonds and velocities, are assigned to the new particles accordingly. Finally, we reduce the length of the resulting box, now containing N_D dendrimers, with the command `fix deform` to obtain the desired box length.

Now we start to equilibrate the system $5 \cdot 10^8$ timesteps followed by 10^8 production timesteps where we calculate and save the following information after every 10^5 timesteps:

- the radius of gyration tensor \mathcal{S} (see Section 5.2.1) for each dendrimer,
- the center of mass \mathbf{R}_{cm} for each dendrimer.

Given these two quantities we can evaluate the following parameters that characterize the shape and orientation of dendrimers in the bulk liquid:

- the radius of gyration R_g , the asphericity b , the acylindricity c , the relative shape anisotropy δ (see section 5.2.1) as well as the ellipsoidal volume V_{ell} given by [54]

$$V_{\text{ell}} = 4\pi\sqrt{3E_1E_2E_3} \quad (6.2)$$

which we normalize by the volume of a sphere V_{sphere} of radius R_g .

- The radial distribution functions $g(r)$ and $g(r, \alpha)$, the orientational order parameter $S(r, \alpha)$ and the conditional probability $P(r, \alpha)$ as described in Sections 5.2 and 5.3. For normalizing the distance we use the results of the radius of gyration of *isolated* (i.e., $\phi_m \approx 0$) D7-type G4 dendrimers $R_g^0 \approx 4.27$ from Ref. [16].

6.1. Shape of D7-type dendrimers (G2 to G8)

We start investigating the shape and size of D7-type dendrimers in the bulk at a packing fraction $\phi_m = 0.248$ and temperature $k_B T = 1.4 \varepsilon_{\text{CC}}^{\text{D7}}$, with the generation number ranging from $G = 2$ (with 14 monomers) up to $G = 8$ (with 1022 monomers). Snapshots of the simulation boxes for different generations of dendrimers are shown in Fig. 6.1, where dendrimers are represented by ellipsoids. The top panel of Fig. 6.2 shows the corresponding results for the radius of gyration R_g , the middle panel displays the asphericity b and acylindricity c and the bottom panel shows the ellipsoidal volume V_{ell} normalized by V_{sphere} and the relative shape anisotropy δ .

In this figure we have also included the respective results of Georgiou et al. [16] for isolated dendrimers of D7-type: the radius of gyration R_g increases with the generation

²<http://lammps.sandia.gov/doc/replicate.html> (online 11.12.2014)

number G and asphericity b as well as acylindricity c decrease with G . We observe similar trends for these quantities in the bulk liquid.

For G2 and G3 all the displayed values for isolated dendrimers and for dendrimers in the bulk are essentially the same. For $G \geq 3$ the radius of gyration is always smaller in the bulk while b and c show only small differences compared to the case of isolated dendrimers. For $G = 6$ we find highly unexpected values for b , V_{ell} and δ which differ significantly from the expected trend while corresponding values of R_g and c nicely follow it. We have made particular efforts to guarantee that the observed effect is indeed reproducible: In order to avoid possible failures due to an unsuitable initial configuration we performed another independent simulation for G6 dendrimers leading to the same results. Further, increasing and decreasing the timespan in which the simulation box is reduced to obtain the desired density did not change the equilibrated values for G6.

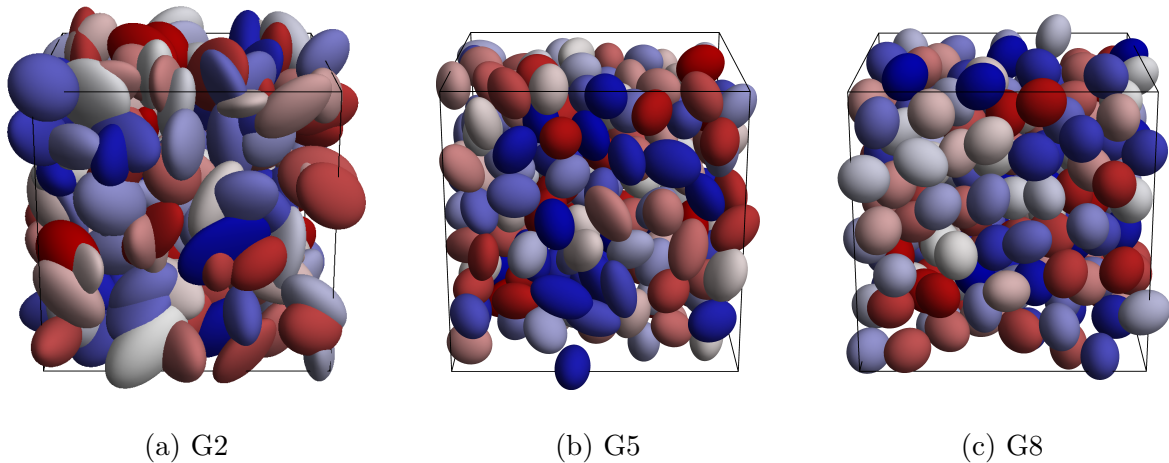


Figure 6.1.: Snapshots of a configuration of 220 D7-type dendrimers of generation G2, G5 and G8, as labeled, at packing fraction $\phi_m = 0.248$ and temperature $k_B T = 1.4 \varepsilon_{CC}^{\text{D7}}$. Dendrimers are represented by ellipsoids as defined in Fig. 5.3b. The coloring is arbitrary. The box lengths are not drawn to scale.

Our most important finding is that the shape of dendrimers in the bulk liquid is also not spherical but rather prolate, similar to isolated dendrimers [16]. In detail, there is a significant change in the shape of dendrimers while going from low to high generations as we can see in Fig. 6.2. Dendrimers of low generations $G = 2$ and $G = 3$ are highly asymmetric, while higher generation dendrimers have nearly spherical shapes.

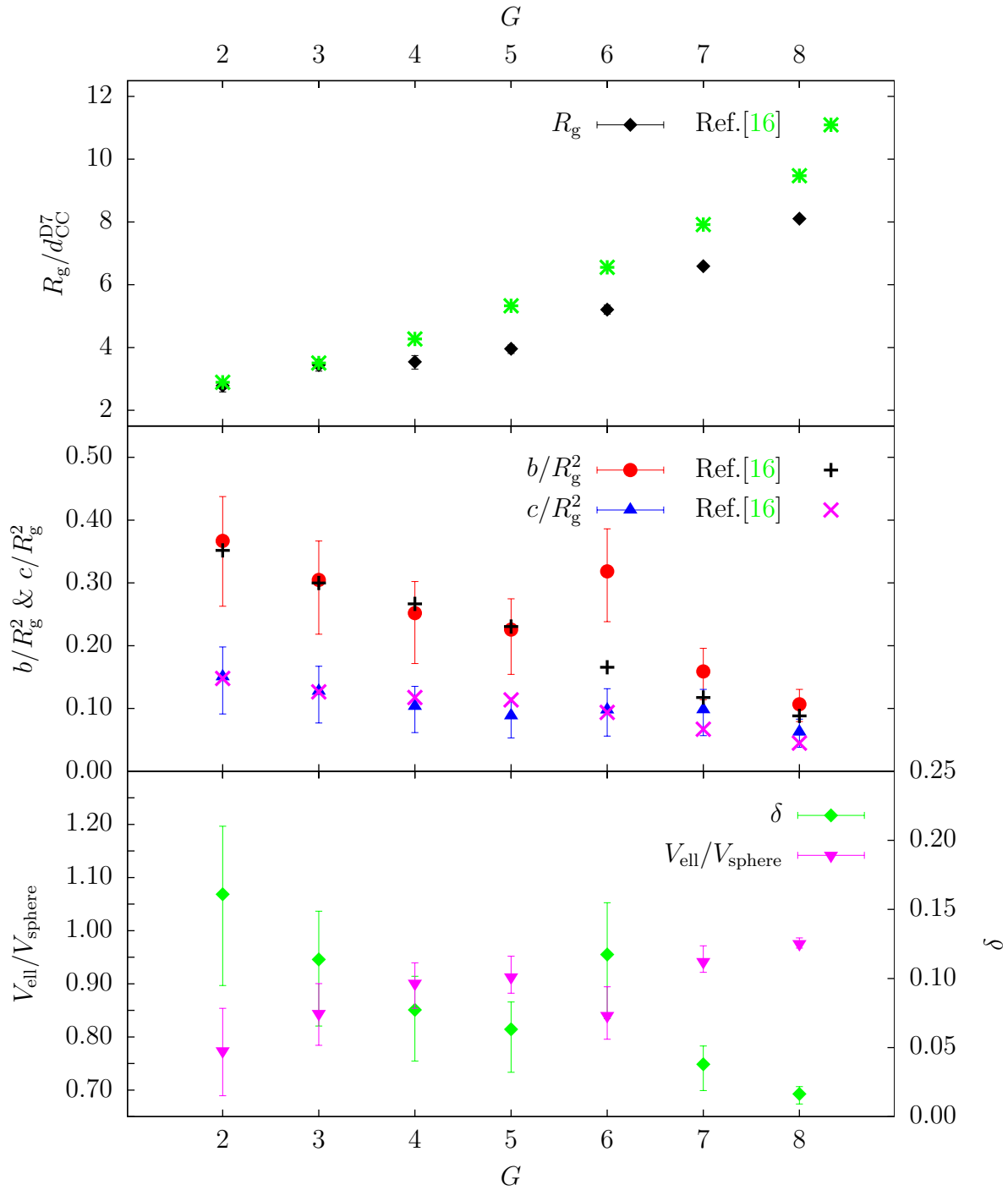


Figure 6.2.: Parameters R_g , b , c , V_{ell} and δ at packing fraction $\phi_m = 0.248$ and temperature $k_B T = 1.4 \varepsilon_{CC}^{D7}$ for D7-type dendrimers as a function of the generation number G . The error bars indicate the first and third quartiles of the corresponding distribution. We also include the results of Georgiou et al. [16] for R_g , b/R_g^2 and c/R_g^2 obtained for isolated dendrimers (i.e., $\phi_m \approx 0$).

6.2. Influence of the packing fraction and of the temperature

In this section we focus on dendrimers of D7-type with a generation number $G = 4$. We are interested in the properties of these molecules in terms of shape and relative orientation considering different temperatures, ranging from $k_B T = 0.7 \varepsilon_{CC}^{D7}$ to $k_B T = 1.8 \varepsilon_{CC}^{D7}$, and three different packing fractions ($\phi_m = 0.248$, $\phi_m = 0.153$ and $\phi_m = 0.095$).

6.2.1. $\phi_m = 0.248$

We start investigating the shape of dendrimers in the bulk liquid at the highest packing fraction $\phi_m = 0.248$ for different temperatures (see snapshots in Fig. 6.3). The obtained results, shown in Fig. 6.4, indicate that the radius of gyration as well as the asphericity b and the relative shape anisotropy δ are increasing with increasing temperature T . Dendrimers at the lowest temperature, i.e. $k_B T = 0.7 \varepsilon_{CC}^{D7}$, are the most spherical molecules and their radius of gyration is the smallest, whereas at the highest temperature, i.e. $k_B T = 1.8 \varepsilon_{CC}^{D7}$, they are strongly aspherical and assume the highest value for R_g ; over this temperature range we observe an increase by around 9%. In contrast, the acylindricity c shows no significant changes while changing temperature. From the bottom panel in Fig. 6.4 we can conclude that the normalized ellipsoidal volume of the dendrimers $V_{\text{ell}}/V_{\text{sphere}}$ is increasing and its value approaches 1 while decreasing temperature, which also indicates more spherical dendrimers.

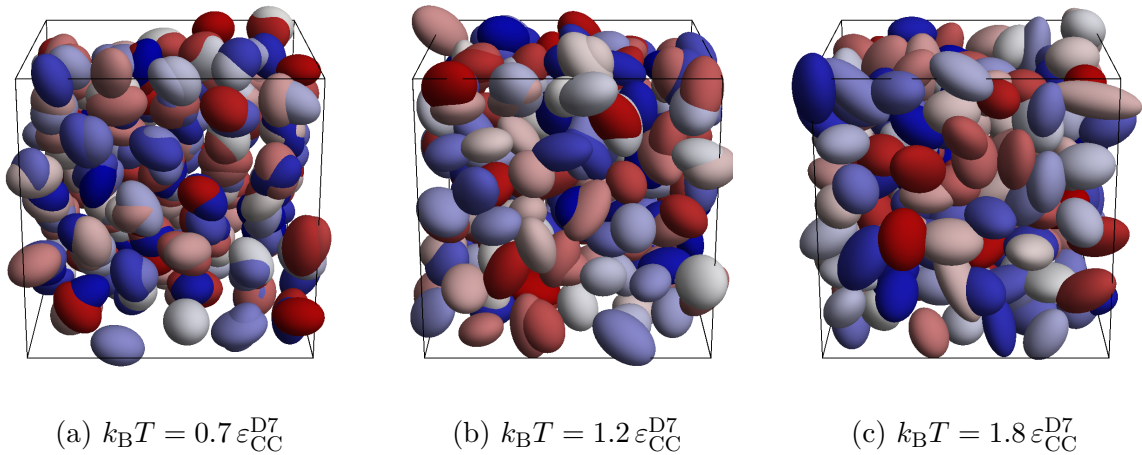


Figure 6.3.: Snapshots of a configuration of 220 G4 dendrimers of D7-type at a volume fraction $\phi_m = 0.248$ and different temperatures, as labeled. Dendrimers are represented by ellipsoids as defined in Fig. 5.3b. The coloring is arbitrary.

In Fig. 6.5 the radial distribution functions $g(r)$ are shown over the temperature range of interest. Already at the lowest temperature we observe that $g(r = 0)$ differs distinctively from zero, indicating that molecules overlap. As T decreases we observe a dramatic

increase of $g(r=0)$, attaining values of ~ 50 . This feature reflects the fact that massive clustering of the molecules occurs at intermediate and low temperatures. Concurrently, as T decreases the respective nearest neighbor peak increases in height and shifts its position to larger r -values.

We now focus on the local spatial and orientational order in the liquid, characterized by the conditional probability $P(r, \alpha)$ and the orientational correlation function $S(r, \alpha)$. For the symbols specifying the relative orientations of the molecules that will be used in the following we refer to Tab. 5.1. Georgiou et al. [16, 22] pointed out that at a packing fraction $\phi_m = 0.248$ and temperature $k_B T = 1.4 \varepsilon_{CC}^{D7}$ dendrimers form a cluster liquid where particles arrange in distinct relative orientations. To be more specific, they showed that dendrimers prefer large- α configurations (— —) at distances $r/R_g^0 \approx 2.5$ and when overlapping $r/R_g^0 \approx 0.25$. In contrast to nearest neighbor dendrimers ($r/R_g^0 \approx 1.5$ and $\alpha < 0.25$) that favor parallel **||** configurations. We can confirm these results within very good agreement and we start to systematically investigate the change in these functions as the temperatures varies.

In order to obtain a comprehensive insight into the spatial and orientational order of the liquid $P(r, \alpha)$ and $S(r, \alpha)$ have to be considered together; their respective contour plots are shown in Fig. 6.6 and Fig. 6.7, respectively. The amount of overlapping dendrimers can be seen from the respective pair distribution function $g(r, \alpha)$ shown in these figures by an isoline specifying a value of 90% of the nearest neighbor peak in $g(r)$; at any given α , the position of the nearest neighbor peak is thus located roughly halfway between the respective small- r and large- r points on the isoline.

Our first observation is a pronounced peak in $P(r, \alpha)$ at $\alpha \approx 1$ for overlapping dendrimers (i.e., at small r/R_g^0) and $0.9 \leq k_B T / \varepsilon_{CC}^{D7} \leq 1.5$ that indicates an end-to-end configuration — — since S is clearly positive. It becomes less distinct for very high ($k_B T = 1.6 \varepsilon_{CC}^{D7}$ and higher) temperatures, where only a low amount of clustering is present. For very low temperatures ($k_B T = 0.7 \varepsilon_{CC}^{D7}$ and $k_B T = 0.8 \varepsilon_{CC}^{D7}$) the peak vanishes, although, a high degree of clustering can be observed. Thus, overlapping dendrimers at these temperatures do not have a clearly preferred value of α .

For low temperatures the peak in $P(r, \alpha)$ at intermediate distances $r/R_g^0 \approx 1.5$ and for $\alpha < 0.25$ is very pronounced; thus nearly all dendrimers at this distances assume a parallel configuration **||**, confirmed by the positive value of $S(r, \alpha)$ in this r - and α -region. At all temperatures intermediate values of α are preferred at distances $r/R_g^0 \approx 2.25$ where S is clearly negative suggesting configurations **I'**, **┐** and **└**. Especially for low temperatures a slight preference for α -values close to unity for $r/R_g^0 \approx 2.8$ indicates again the occurrence of end-to-end configuration — —. Taking the results from [16] for the effective interaction, this distance corresponds to the onset of the dendrimer-dendrimer interaction.

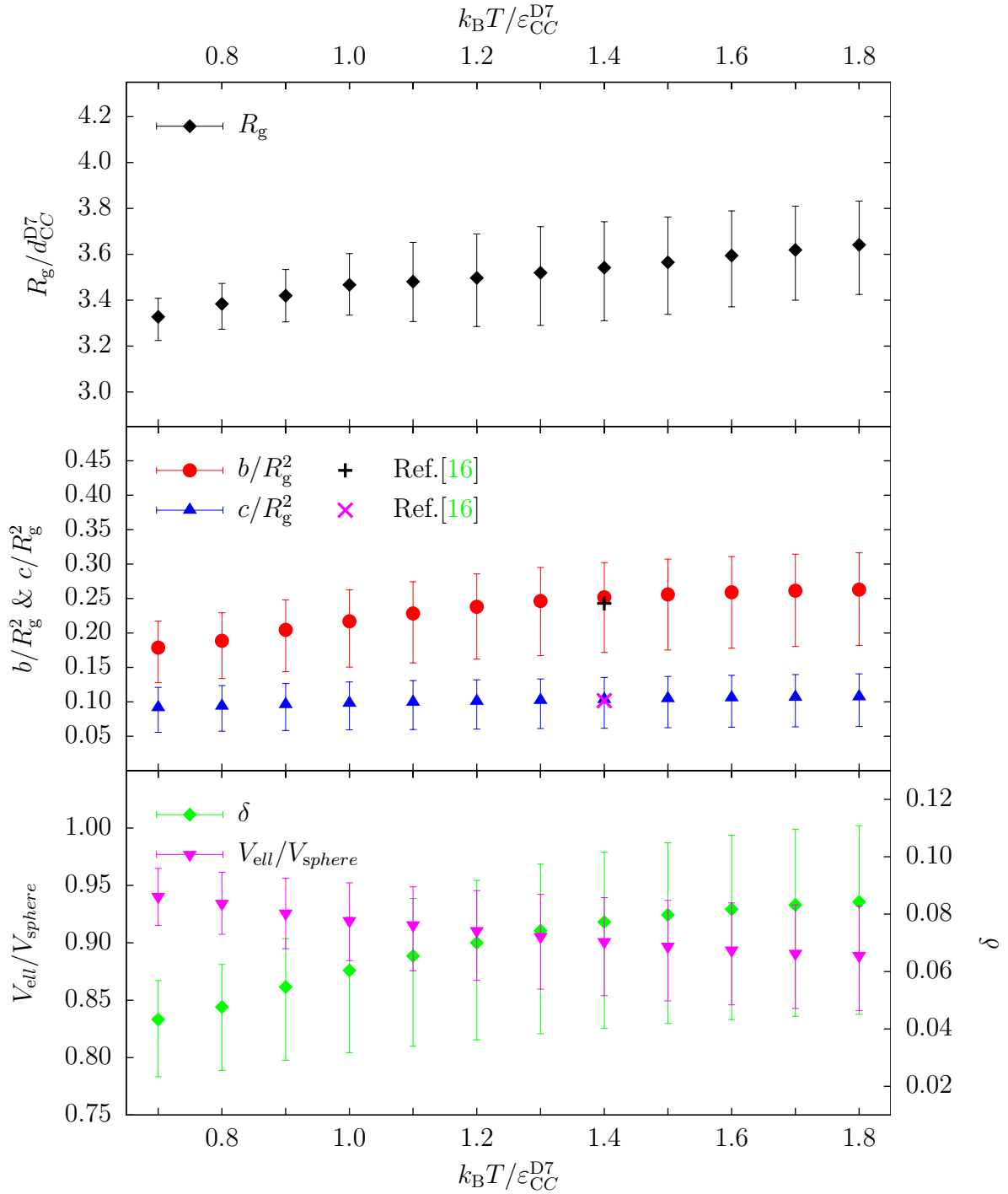


Figure 6.4.: Parameters R_g , b , c , V_{ell} and δ for G4 D7-type dendrimers at packing fraction $\phi_m = 0.248$ as a function of temperature T . The error bars indicate the first and third quartiles of the corresponding distribution. We also include the results of Georgiou et al. [16] for b / R_g^2 and c / R_g^2 obtained for exactly the same system at $k_B T = 1.4 \varepsilon_{CC}^{\text{D7}}$.

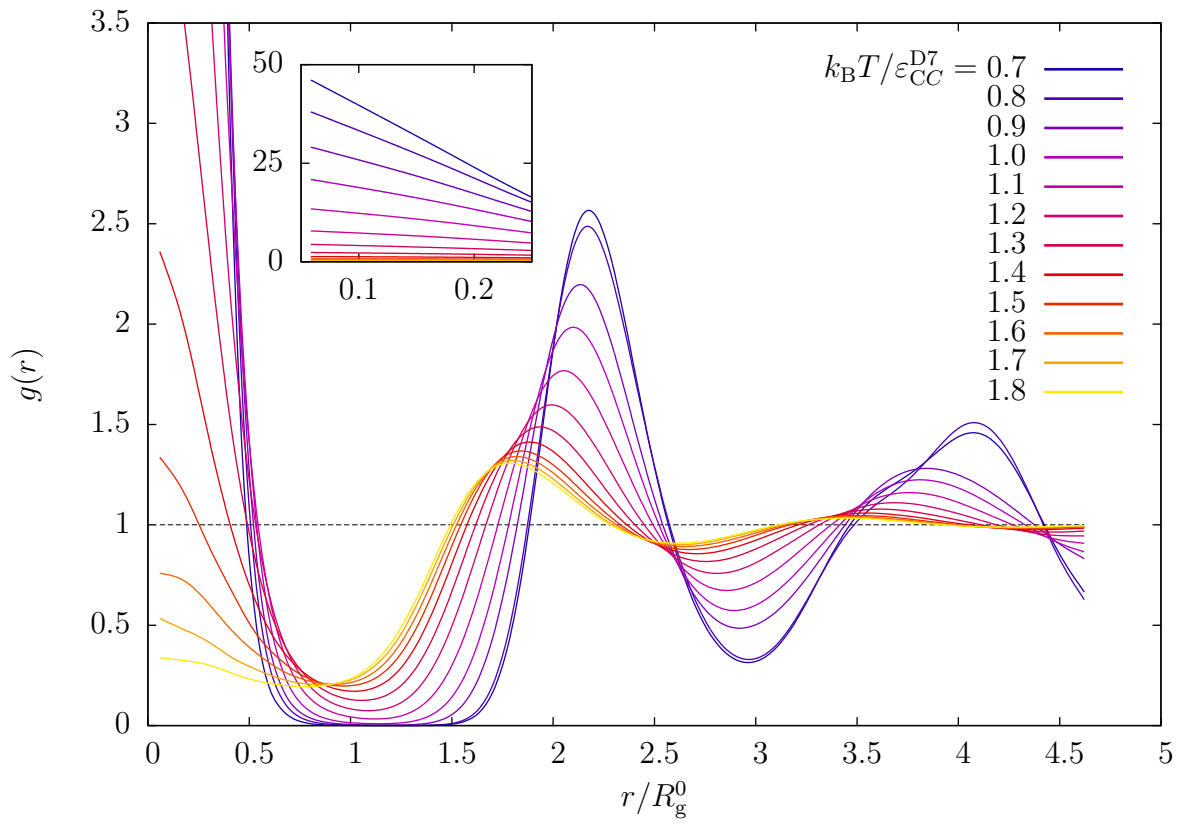


Figure 6.5.: Pair distribution functions $g(r)$ for G4 D7-type dendrimers at packing fraction $\phi_m = 0.248$ and temperatures T as labeled. The inset shows the full range of the functions at small distances.

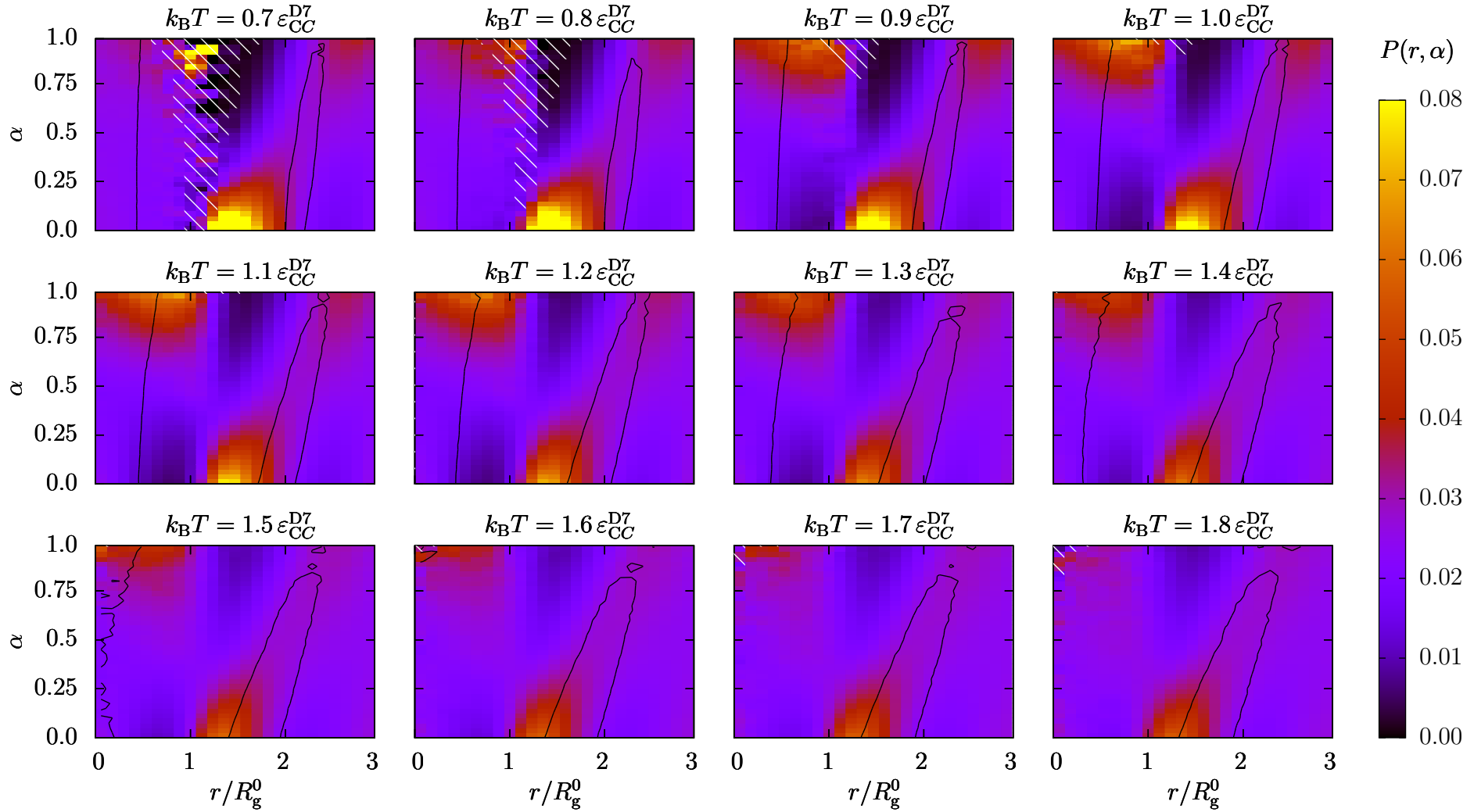


Figure 6.6.: Contour plots of the conditional probability $P(r, \alpha)$ for G4 D7-type dendrimers at packing fraction $\phi_m = 0.248$ and temperature T as labeled. The color scale is shown at the right-hand side of the diagrams. The black isolines indicate where the pair distribution function $g(r, \alpha)$ attains 90% of the height of the nearest-neighbor peak. (r, α) -values with less than 10 realizations are superposed by diagonal lines colored in white.

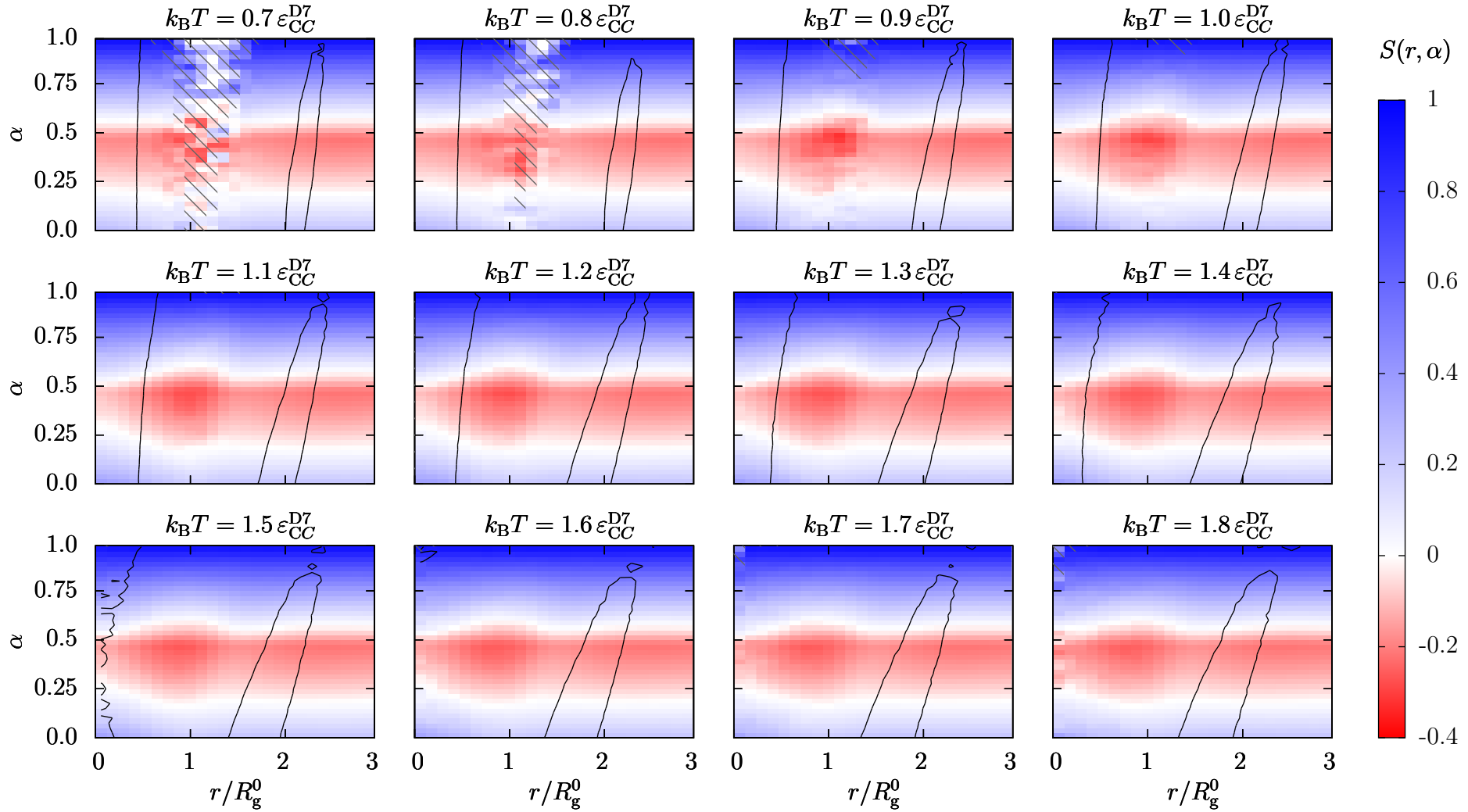


Figure 6.7.: Contour plots of the orientational order parameter $S(r, \alpha)$ for G4 D7-type dendrimers at packing fraction $\phi_m = 0.248$ and temperature T as labeled. The color scale is shown at the right-hand side of the diagrams. The black isolines indicate where the pair distribution function $g(r, \alpha)$ attains 90% of the height of the nearest-neighbor peak. (r, α) -values with less than 10 realizations are superposed by diagonal lines colored in gray.

6.2.2. $\phi_m = 0.153$

Now we investigate the shape of dendrimers in a bulk at a smaller packing fraction $\phi_m = 0.153$ for different temperatures (see snapshots in Fig. 6.8). From Fig. 6.9, where the obtained results are shown, we see that R_g increases by nearly 20% when comparing its values at the lowest temperature $k_B T = 0.7 \varepsilon_{CC}^{D7}$ and the highest temperature $k_B T = 1.8 \varepsilon_{CC}^{D7}$. Thus, at this packing fraction the radius of gyration R_g of the dendrimers is more affected by temperature changes compared to the case of $\phi_m = 0.248$ (see subsection 6.2.1). The overall trend to a less spherical, regarding b , $V_{\text{ell}}/V_{\text{sphere}}$ and δ , and bigger shape, in terms of R_g , while increasing temperature remains and is even more pronounced. However, the acylindricity shows only a slight and irrelevant increase while raising temperature.

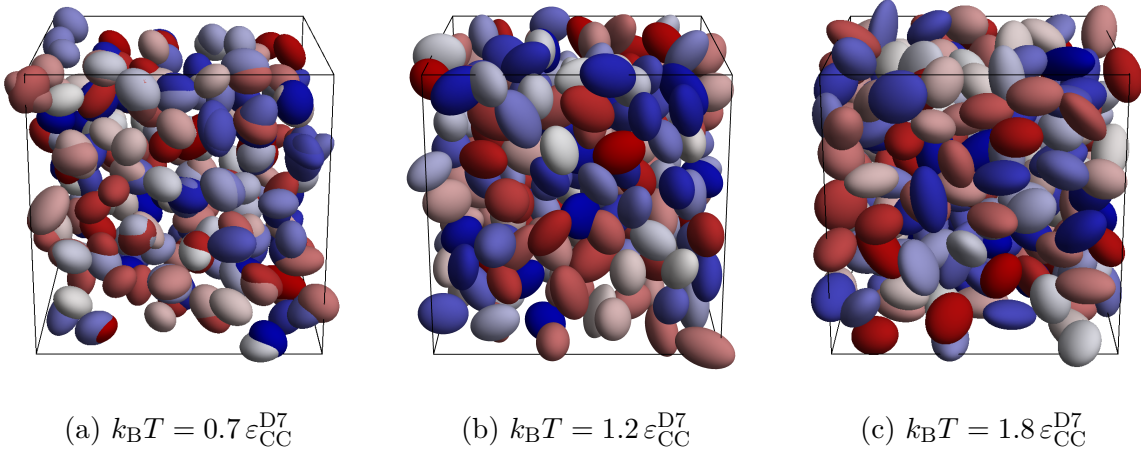


Figure 6.8.: Snapshots of a configuration of 220 G4 dendrimers of D7-type at a volume fraction $\phi_m = 0.153$ and different temperatures as labeled. Dendrimers are represented by ellipsoids as defined in Fig. 5.3b. The coloring is arbitrary.

From the radial distribution functions, shown in Fig. 6.10, we can conclude that the value $g(r = 0)$ is generally smaller as compared to the denser packing fraction $\phi_m = 0.248$ (see subsection 6.2.1). Here only for temperatures lower than $k_B T = 1.0 \varepsilon_{CC}^{D7}$ a considerable amount of overlapping dendrimers can be observed and $g(r = 0)$ attains values of ~ 30 . For higher temperatures the value of $g(r = 0)$ is close to zero, indicating that clustering is rare. As for $\phi_m = 0.248$, we observe a similar tendency in the position and the height of the nearest neighbor peak to smaller r -values and lower values of $g(r)$ when increasing temperature.

From the results for $P(r, \alpha)$ and $S(r, \alpha)$, shown in Fig. 6.11 and Fig. 6.12, we conclude that overlapping dendrimers (i.e., $r/R_g^0 \approx 0.2$) prefer $\alpha \approx 1$ which indicates an end-to-end configuration --- . For all temperatures we find another distinct maximum in $P(r, \alpha)$ for $\alpha < 0.25$ and at temperature dependent distances $r/R_g^0 \approx 1.0 - 1.9$, implying parallel || configurations. Again at all temperatures, intermediate values of α are preferred at distances $r/R_g^0 \approx 2.25$ where S is clearly negative suggesting configurations !^\bullet , ! and

L. At distances $r/R_g^0 \approx 2.8$ a slight preference for α -values close to unity indicates the occurrence of end-to-end configuration **— —**.

By comparing our findings at packing fractions $\phi_m = 0.248$ and $\phi_m = 0.153$, we find that both the preference of end-to-end configuration **— —** for overlapping dendrimers (if present) and the preference of parallel configuration **||** at intermediate distances are distinctively more pronounced in the case of a more dilute system.

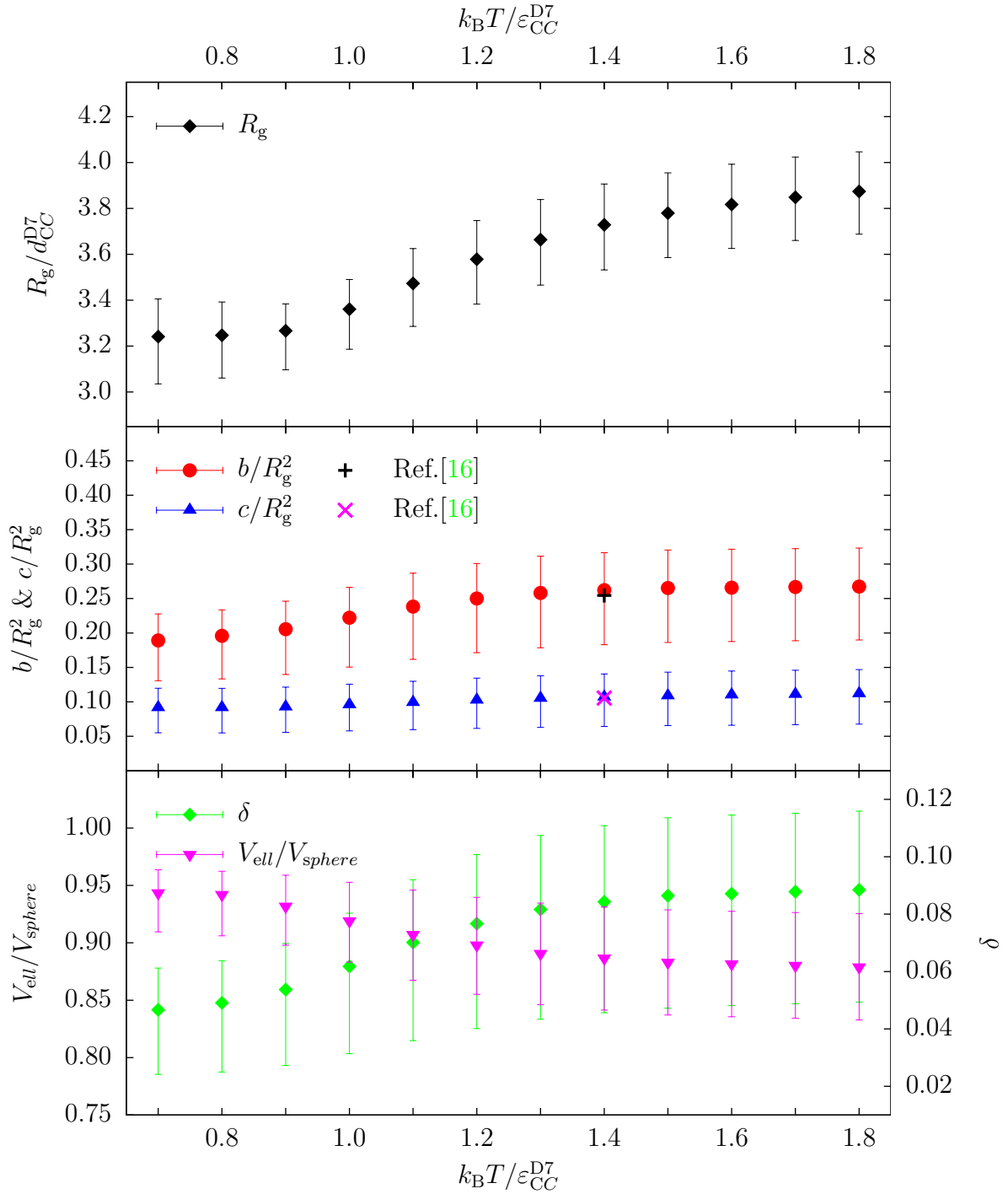


Figure 6.9.: Parameters R_g , b , c , V_{ell} and δ for G4 D7-type dendrimers at packing fraction $\phi_m = 0.153$ as a function of temperature T . The error bars indicate the first and third quartiles of the corresponding distribution. We also include the results of Georgiou et al. [16] for b/R_g^2 and c/R_g^2 obtained for exactly the same system at $k_B T = 1.4 \epsilon_{CC}^{D7}$.

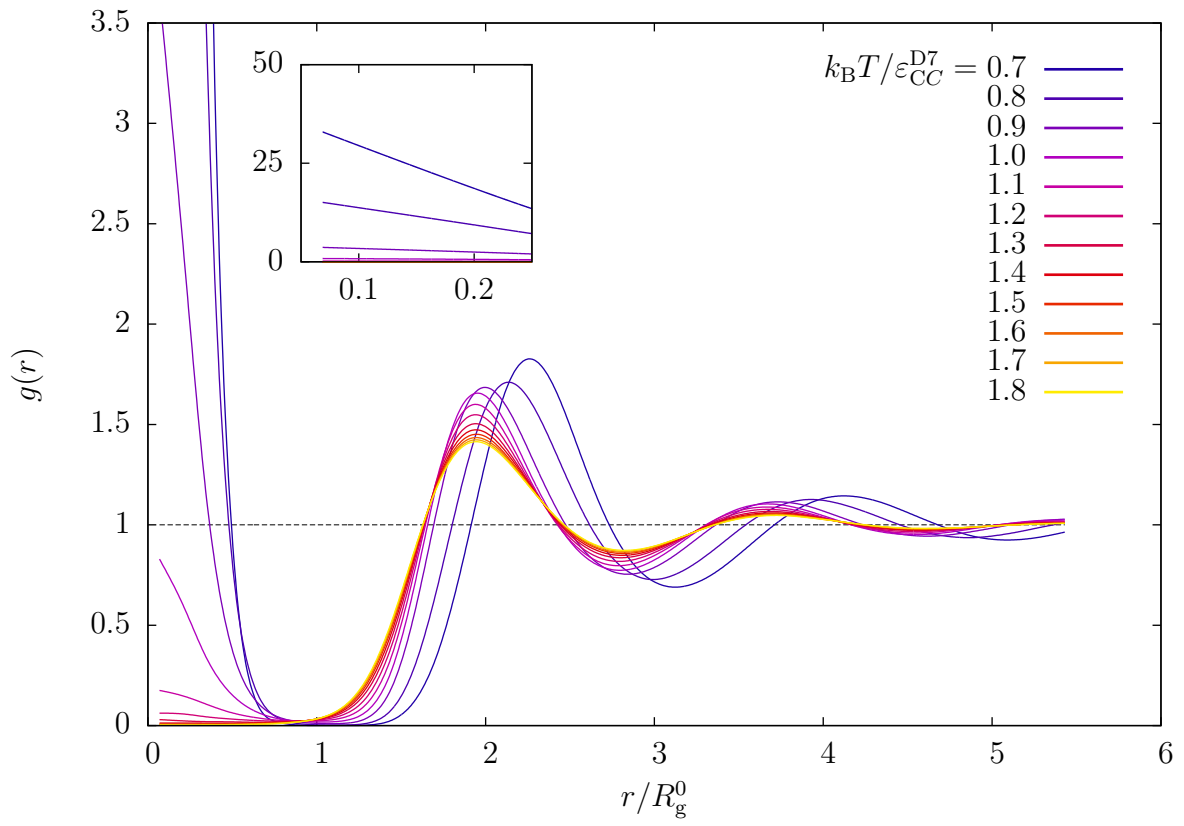


Figure 6.10.: Pair distribution functions $g(r)$ for G4 D7-type dendrimers at packing fraction $\phi_m = 0.153$ and temperatures T as labeled. The inset shows the full range of the functions at small distances.

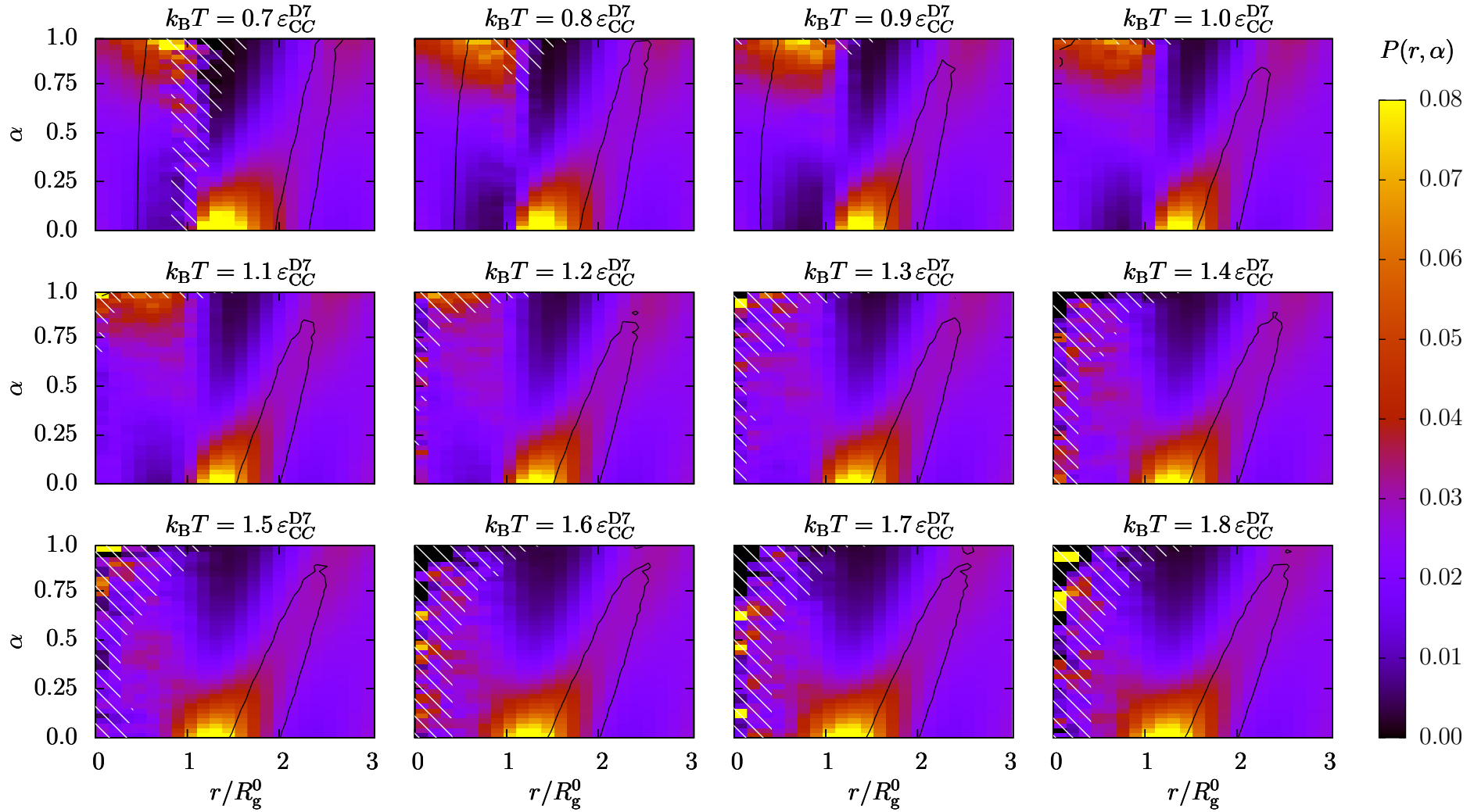


Figure 6.11.: Contour plots of the conditional probability $P(r, \alpha)$ for G4 D7-type dendrimers at packing fraction $\phi_m = 0.153$ and temperature T as labeled. The color scale is shown at the right-hand side of the diagrams. The black isolines indicate where the pair distribution function $g(r, \alpha)$ attains 90% of the height of the nearest-neighbor peak. (r, α) -values with less than 10 realizations are superposed by diagonal lines colored in white.

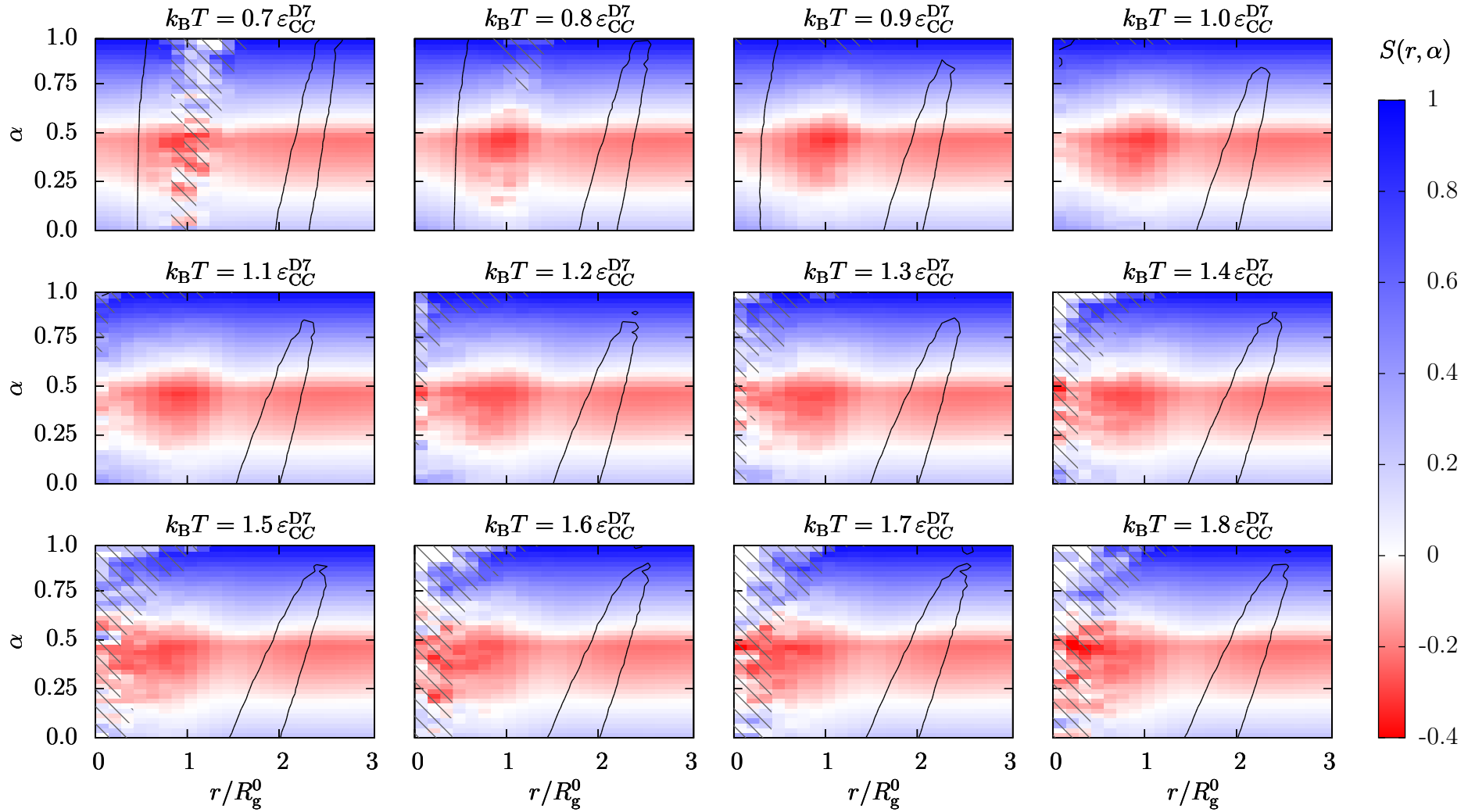


Figure 6.12.: Contour plots of the orientational order parameter $S(r, \alpha)$ for G4 D7-type dendrimers at packing fraction $\phi_m = 0.153$ and temperature T as labeled. The color scale is shown at the right-hand side of the diagrams. The black isolines indicate where the pair distribution function $g(r, \alpha)$ attains 90% of the height of the nearest-neighbor peak. (r, α) -values with less than 10 realizations are superposed by diagonal lines colored in gray.

6.2.3. $\phi_m = 0.095$

The results of the shape analysis of a bulk system of dendrimers for the smallest packing fraction $\phi_m = 0.095$ and different temperatures are presented in Fig. 6.14. We see that for the highest temperature, i.e. $k_B T = 1.8 \varepsilon_{CC}^{D7}$, R_g is 32% larger compared to the value at the lowest temperature, i.e. $k_B T = 0.7 \varepsilon_{CC}^{D7}$. Hence, we observe that the radius of gyration R_g of the dendrimers at this packing fraction is even more affected by temperature changes compared to $\phi_m = 0.153$ (see Sec. 6.2.2). The asphericity, in terms of b , $V_{\text{ell}}/V_{\text{sphere}}$ and δ grows with increasing temperature and reaches a plateau at $k_B T = 1.1 \varepsilon_{CC}^{D7}$. The central panel of Fig. 6.14 shows only a slight and negligible increase in acylindricity while raising temperature.

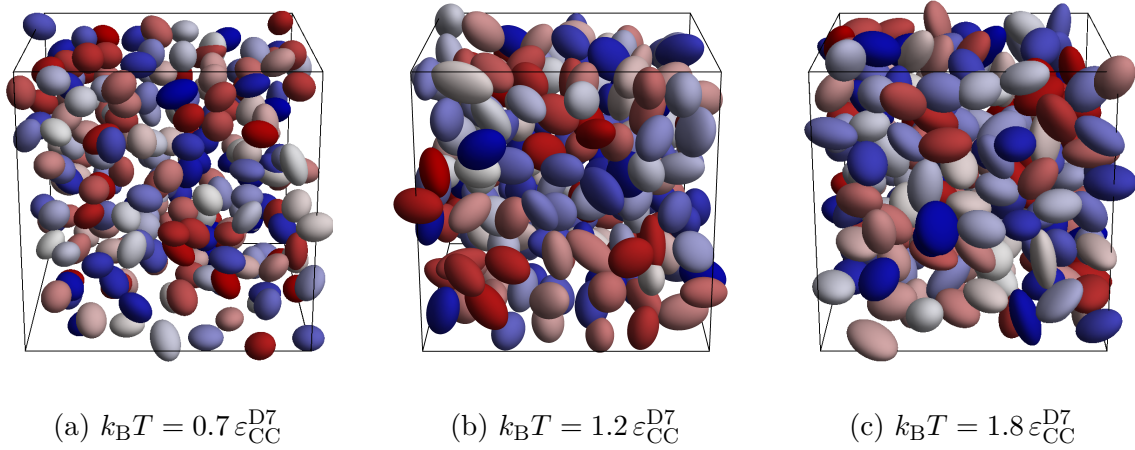


Figure 6.13.: Snapshots of a configuration of 220 G4 dendrimers of D7-type at a volume fraction $\phi_m = 0.095$ and different temperatures as labeled. Dendrimers are represented by ellipsoids as defined in Fig. 5.3b. The coloring is arbitrary.

Although, the radial distribution function (see Fig. 6.15) is nearly identical on a wide range of r/R_g^0 for all temperatures, we find a considerable amount of overlapping dendrimers in the case of $k_B T = 0.7 \varepsilon_{CC}^{D7}$, the lowest temperature. Here $g(r=0)$ attains only about 2.25 times the height of the nearest neighbor peak and we can verify our finding that the value $g(r=0)$ is decreasing with decreasing packing fraction (see subsection 6.2.2).

We now focus on the local orientational order, characterized by the conditional probability $P(r, \alpha)$, shown in Fig. 6.16, and the orientational correlation function $S(r, \alpha)$, shown in Fig. 6.17. Overlapping dendrimers are only observed for $k_B T = 0.7 \varepsilon_{CC}^{D7}$ where we find similar results for the relative orientation as for $\phi_m = 0.153$ and at a similar temperature (see Sec. 6.2.2). Thus, we concentrate on the results for higher temperatures: There is a distinct peak in $P(r, \alpha)$ at intermediate distances $r/R_g^0 \approx 1.5$ and low values of $\alpha < 0.25$; thus nearly all dendrimers at this distance assume a parallel configuration II, since $S(r, \alpha)$ is positive at these r - and α -values. Again intermediate values of α are preferred at distances $r/R_g^0 \approx 2.25$ where $S(r, \alpha)$ is clearly negative, suggesting configu-

ratios \mathbf{I}^\bullet , \mathbf{L} and \mathbf{L} . For all temperatures we find a slight preference for α -values close to unity at $r/R_g^0 \approx 2.8$ indicating the presents of an end-to-end configuration $\mathbf{--}$.

By comparing our findings with those for packing fractions $\phi_m = 0.248$ and $\phi_m = 0.153$ (Sec. 6.2.1 and 6.2.2), we conclude that the preference of parallel configurations $\mathbf{||}$ is more pronounced over a wider range of intermediate distances.

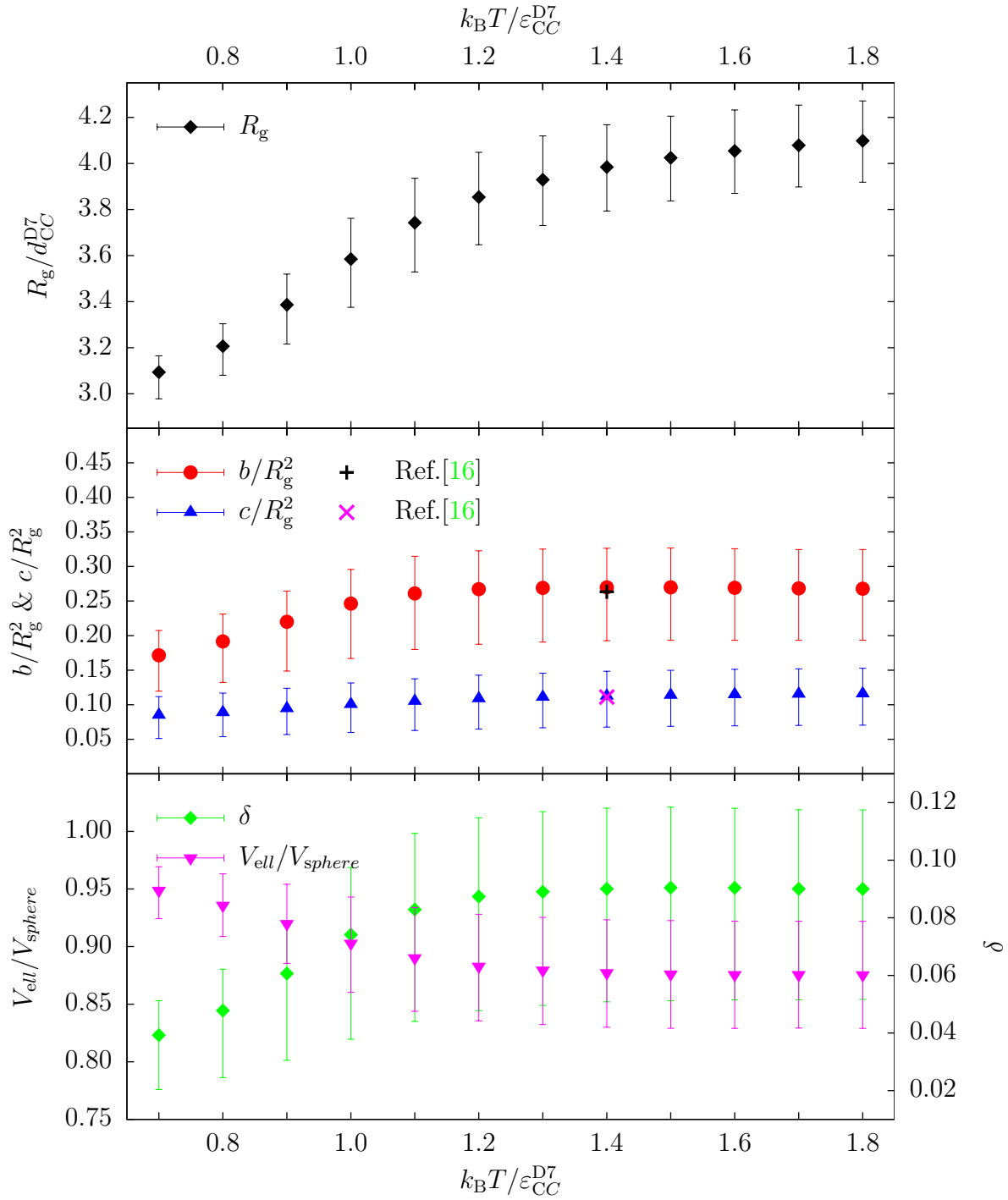


Figure 6.14.: Parameters R_g , b , c , V_{ell} and δ for G4 D7-type dendrimers at packing fraction $\phi_m = 0.095$ as a function of temperature T . The error bars indicate the first and third quartiles of the corresponding distribution. We also include the results of Georgiou et al. [16] for b/R_g^2 and c/R_g^2 obtained for exactly the same system at $k_B T = 1.4 \epsilon_{CC}^{\text{D7}}$.

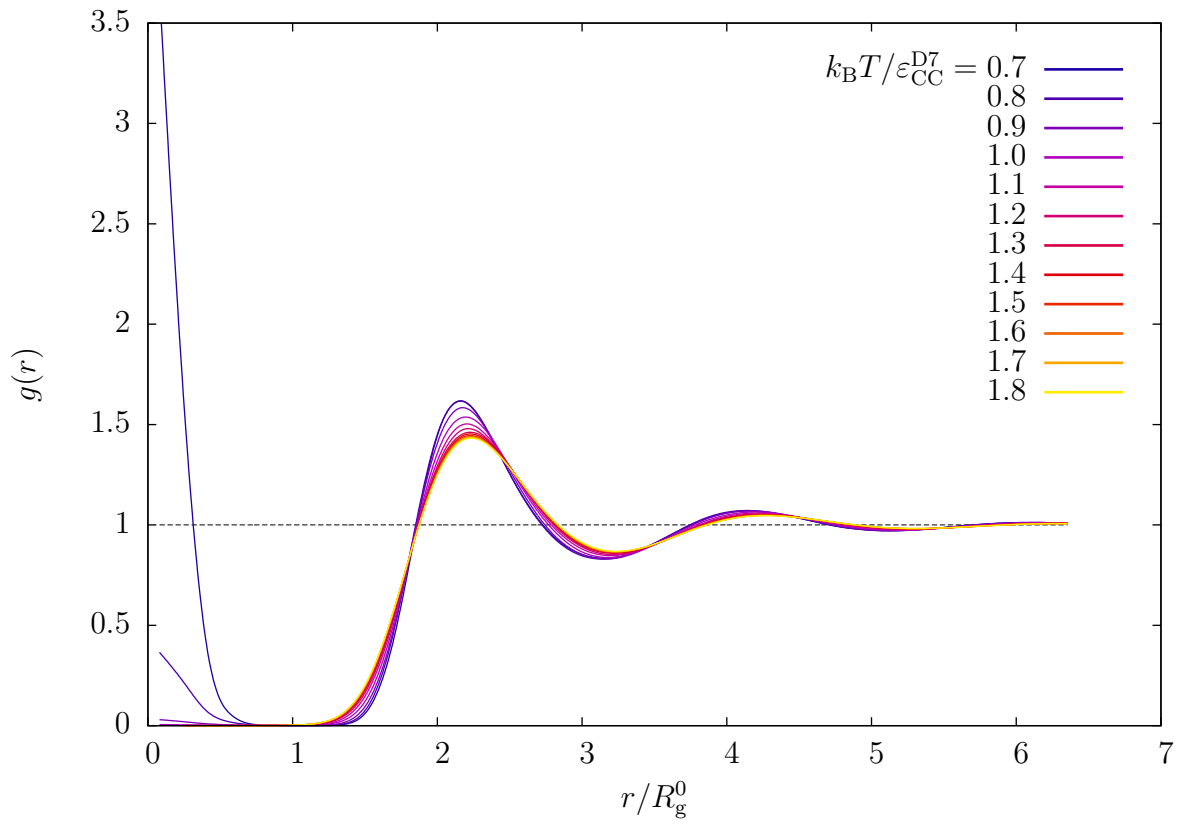


Figure 6.15.: Pair distribution functions $g(r)$ for G4 D7-type dendrimers at packing fraction $\phi_m = 0.095$ and temperatures T as labeled.

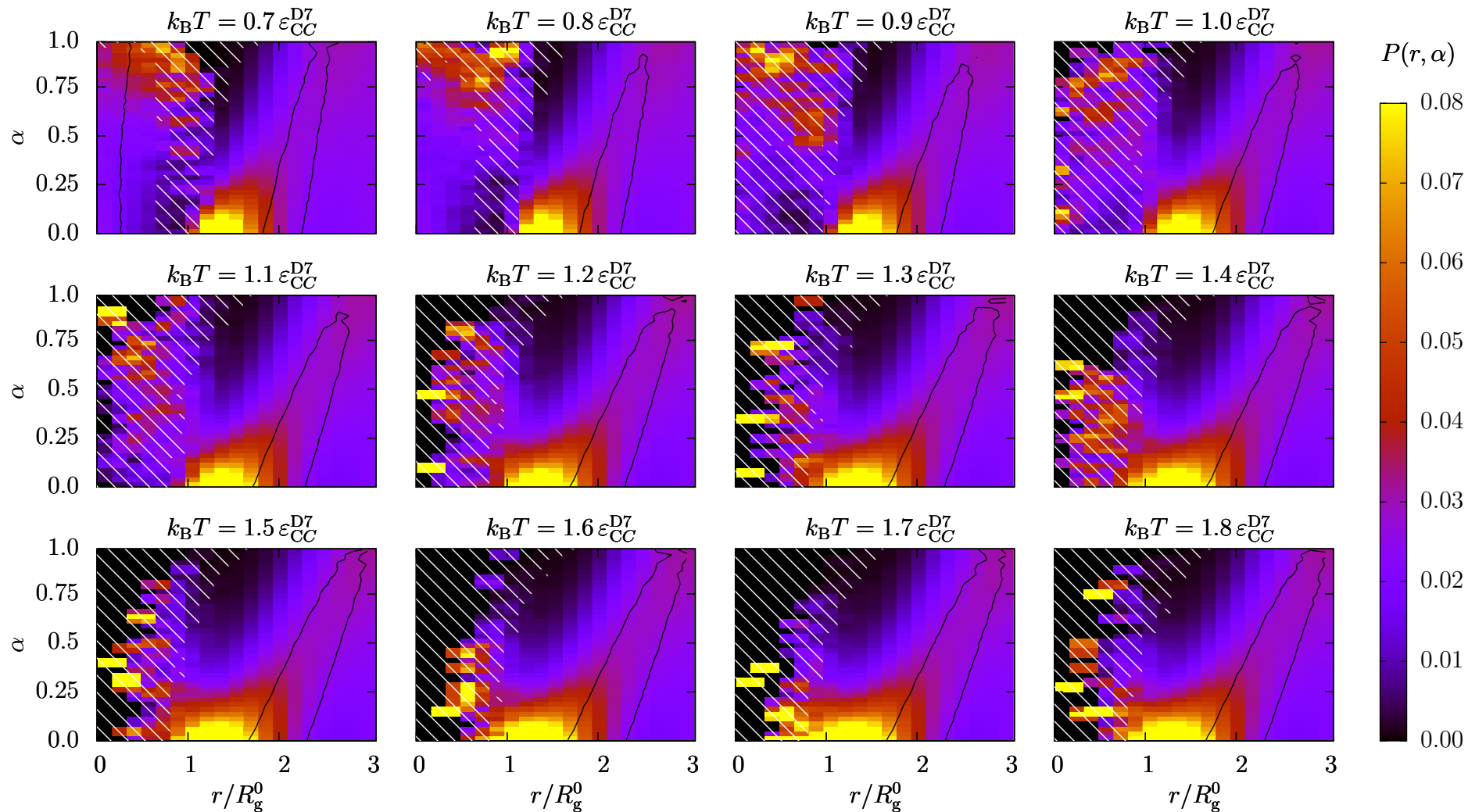


Figure 6.16.: Contour plots of the conditional probability $P(r, \alpha)$ for G4 D7-type dendrimers at packing fraction $\phi_m = 0.095$ and temperature T as labeled. The color scale is shown at the right-hand side of the diagrams. The black isolines indicate where the pair distribution function $g(r, \alpha)$ attains 90% of the height of the nearest-neighbor peak. (r, α) -values with less than 10 realizations are superposed by diagonal lines colored in white.

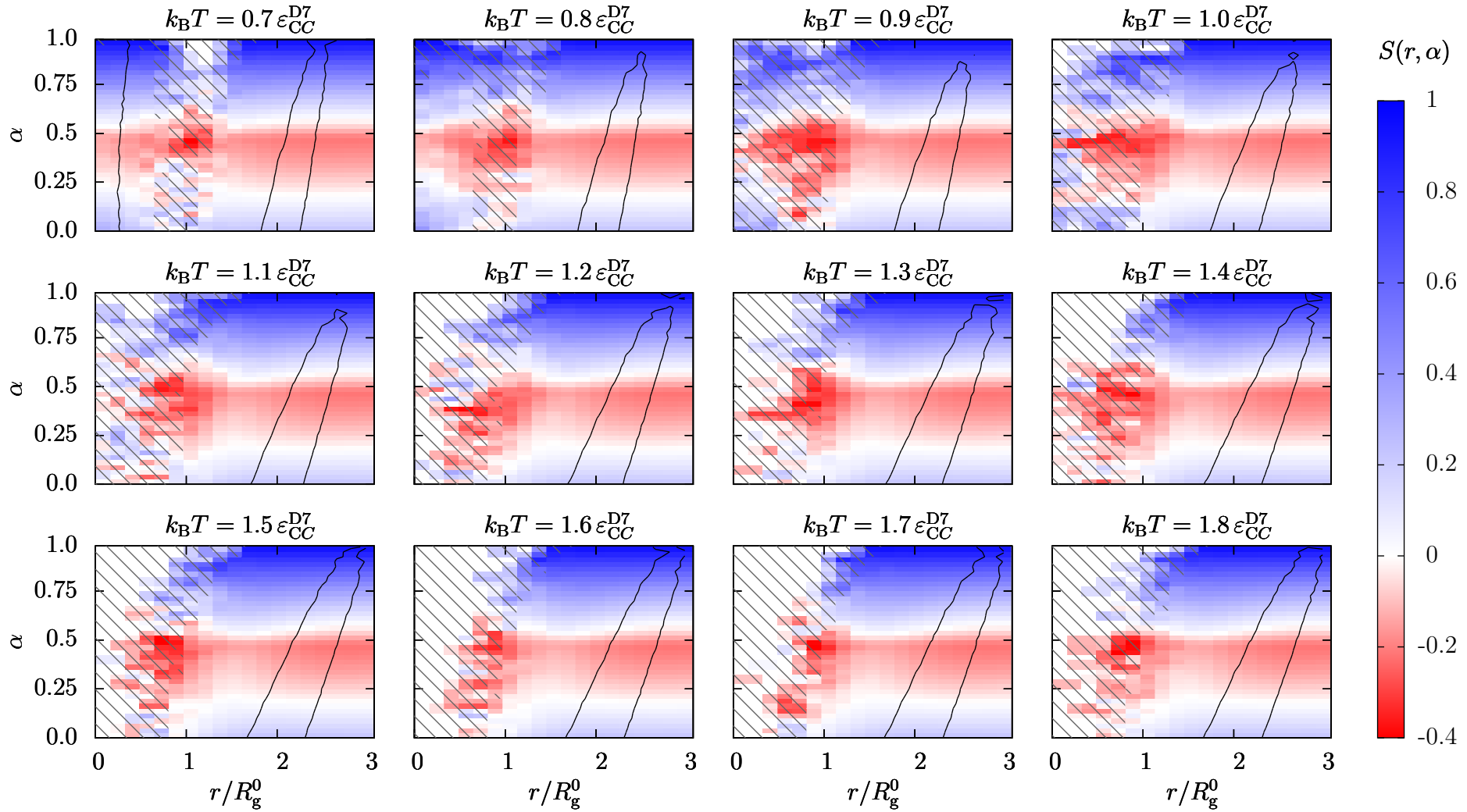


Figure 6.17.: Contour plots of the orientational order parameter $S(r, \alpha)$ for G4 D7-type dendrimers at packing fraction $\phi_m = 0.095$ and temperature T as labeled. The color scale is shown at the right-hand side of the diagrams. The black isolines indicate where the pair distribution function $g(r, \alpha)$ attains 90% of the height of the nearest-neighbor peak. (r, α) -values with less than 10 realizations are superposed by diagonal lines colored in gray.

6.3. Tuning amphiphilicity

In this section we investigate the shape and orientation in the dendrimer liquid at packing fraction $\phi_m = 0.248$ and temperature $k_B T = 1.4 \varepsilon_{CC}^{D7}$ for different types of dendrimers X1 ($x = 0.00$), X2 ($x = 0.25$), X3 ($x = 0.50$), X4 ($x = 0.75$), X5 ($x = 0.90$), X6 ($x = 0.95$) and D7 ($x = 1.00$) in order of increasing amphiphilicity, as described in Sec. 3.2.1. With decreasing amphiphilicity (parametrized by x) the difference in core and shell monomers diminishes until it vanishes for X1 ($x = 0.00$). The detailed parameters for each type of dendrimer are given in Appendix A. Snapshots of the simulation boxes of three different types of dendrimers are shown in Fig. 6.18, where dendrimers are represented by ellipsoids, as described in Fig. 5.3b.

By examining the results of the shape analysis of the different types of dendrimers, shown in Fig. 6.19, we find that the radius of gyration is decreasing nearly linearly with increasing amphiphilicity parameter x . This is due to the linear decrease of the core-core bond length from X1 ($x = 0.00$) to D7 ($x = 1.00$). Whereas the asphericity, in terms of b/R_g^2 and δ , and acylindricity c of X1-, X2-, X3-, X4- and X5-type dendrimers show only a slight decrease with increasing x , they change significantly for X6- and X7-type dendrimers. In conclusion, dendrimers become more spherical and slightly more cylindrical with increasing amphiphilicity.

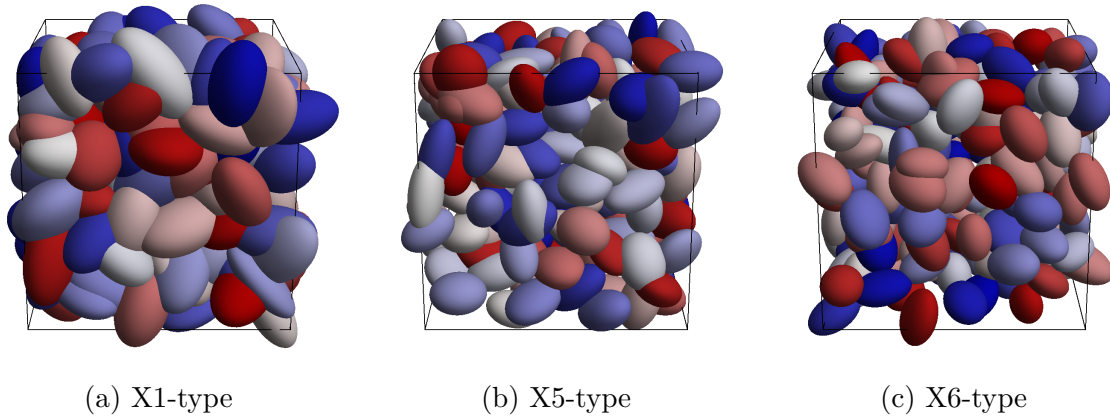


Figure 6.18.: Snapshots of a configuration of 220 G4 dendrimers at a volume fraction $\phi_m = 0.248$ and temperature $k_B T = 1.4 \varepsilon_{CC}^{D7}$; interaction type as labeled. Dendrimers are represented by ellipsoids as defined in Fig. 5.3b. The coloring is arbitrary.

However, not only the shape of the dendrimers changes, also the radial distribution function (shown in Fig. 6.20) undergoes a transition due to the tuning of the amphiphilic behavior. The most remarkable change can be found for $g(r = 0)$, where only D7 ($x = 1.00$) shows considerable amount of overlapping dendrimers. In the case of X6 ($x = 0.95$) $g(r = 0)$ is already smaller than at the nearest neighbor peak and only a small amount of dendrimers is overlapping. Also, the radial distribution function for $r/R_g^0 > 1.5$ flattens and approaches that of randomly distributed particles $g(r) = 1$ while increasing amphiphilicity, in terms of x .

Based on the results of shape and radial distribution, we also expect fundamental changes in the relative orientation of dendrimers in the bulk liquid. When analyzing Fig. 6.21 and Fig. 6.22, we find that the characteristic peak in $P(r, \alpha)$ of D7-type ($x = 1.00$) dendrimers at distance $r/R_g^0 \approx 0.25$ and $\alpha \approx 1$ (indicating a --- alignment since S is positive) is less pronounced for X6 ($x = 0.95$) and hardly noticeable for X5 ($x = 0.90$) while the other types of dendrimers rather show low values of α (< 0.5) at these distances. At intermediate distances $r/R_g^0 \approx 1.0 - 1.5$ X5, X6 and D7 favor parallel configurations || since S is positive. In the case of X1 ($x = 0.00$), X2 ($x = 0.25$), X3 ($x = 0.50$) and X4 ($x = 0.75$) the range where parallel configurations || are preferred becomes wider $r/R_g^0 \approx 0.25 - 1.5$. X1-, X2- and, to some degree, X3-type dendrimers show no significant relative orientation for distances $r/R_g^0 > 2.0$, while X4-, X5-, X6- and D7-type dendrimers favor configurations I' , ┐ and └ at intermediate values of α and at distances $r/R_g^0 \approx 2.25$. For the latter interaction types a slight preference for α -values close to unity for $r/R_g^0 \approx 2.8$ indicates again the occurrence of end-to-end configuration --- .

To summarize, dendrimers with strong amphiphilic character tend to a complex order where the relative orientation strictly depends on the dendrimer-dendrimer distance, whereas dendrimers where the interactions of core and shell monomers are less disparate show a rather simple order where only nearby dendrimers do not arrange randomly.

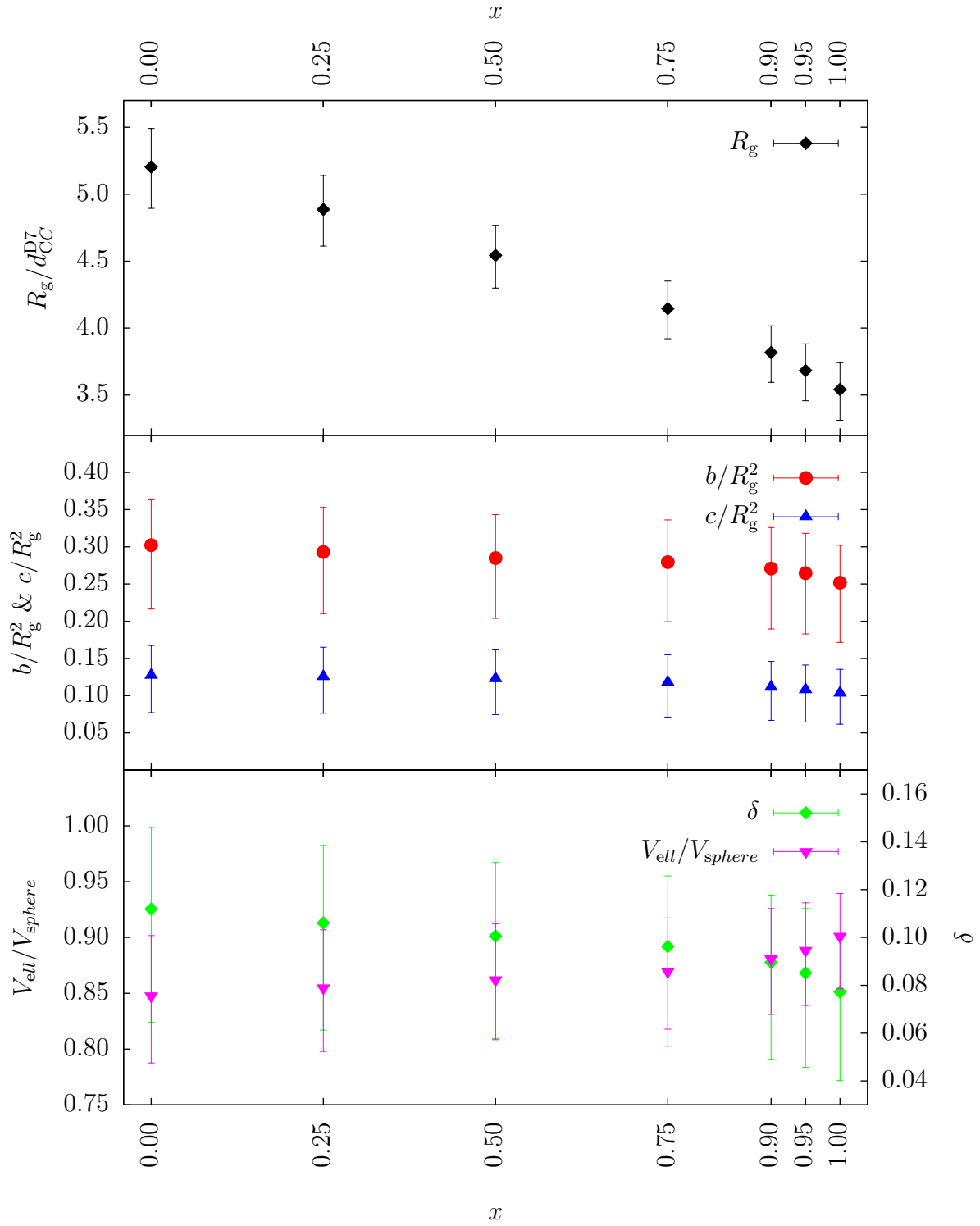


Figure 6.19.: Parameters R_g , b , c , V_{ell} and δ at packing fraction $\phi_m = 0.248$ and temperature $k_B T = 1.4 \varepsilon_{CC}^{D7}$ as a function of x (i.e., a parameter for the amphiphilicity of the dendrimers; see Sec. 3.2.1). The error bars indicate the first and third quartiles of the corresponding distribution.

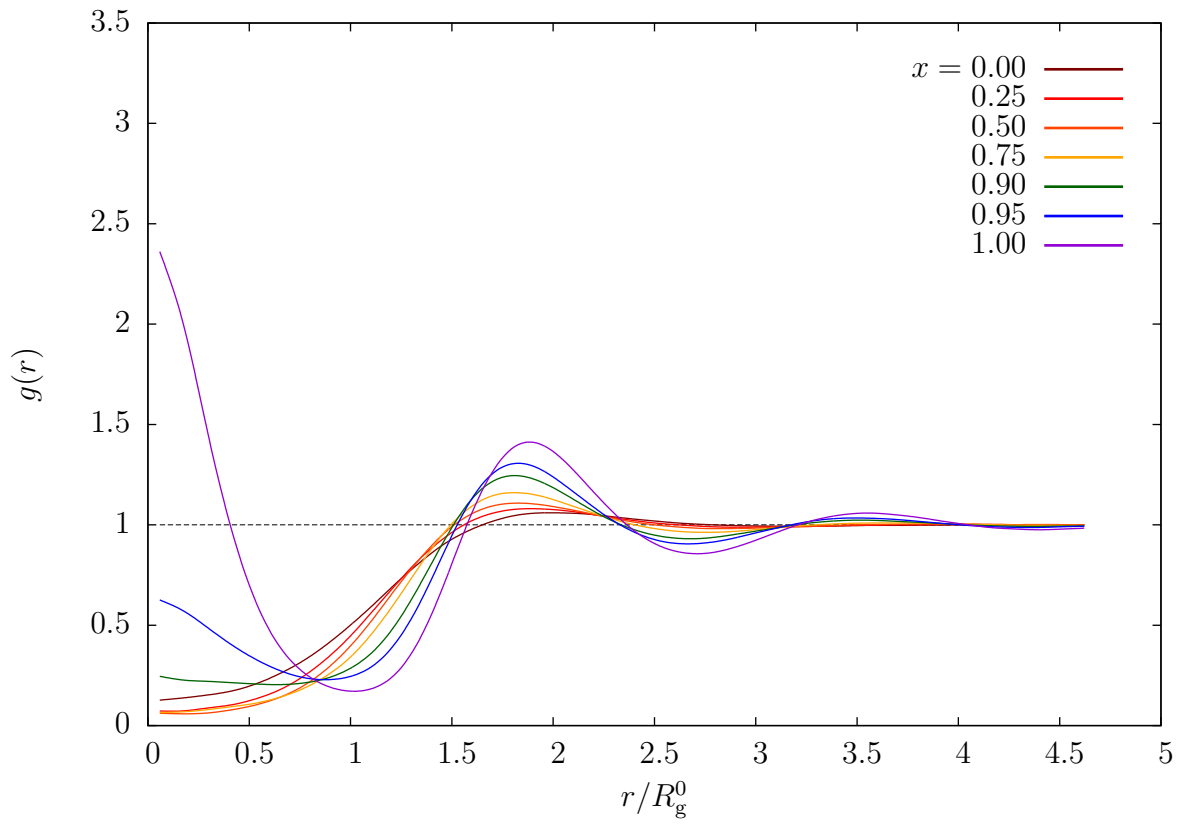


Figure 6.20.: Pair distribution functions $g(r)$ at packing fraction $\phi_m = 0.248$, temperature $k_B T = 1.4 \varepsilon_{CC}^{D7}$ and x as labelled (i.e., a parameter for the amphiphilicity of the dendrimers; see Sec. 3.2.1).

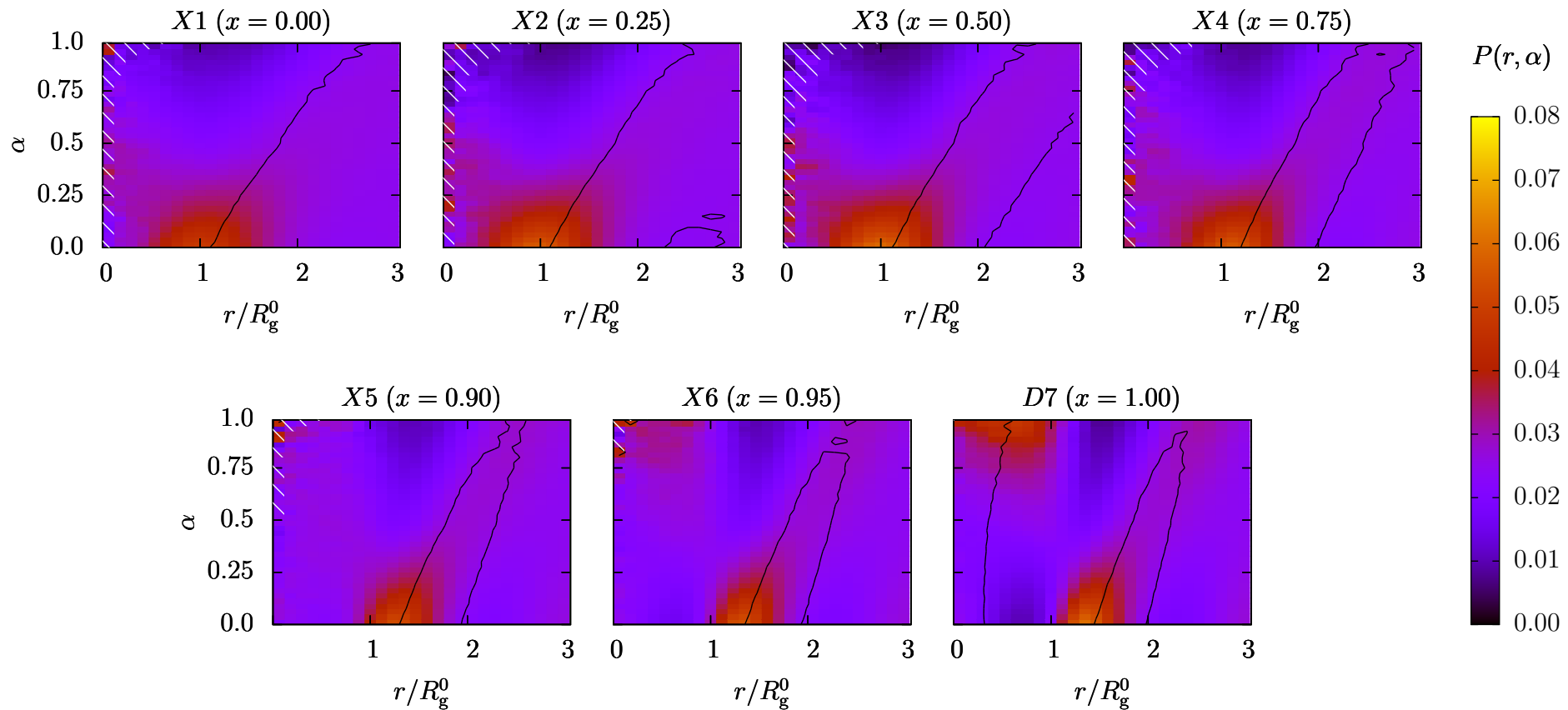


Figure 6.21.: Contour plots of the conditional probability $P(r, \alpha)$ for G4 dendrimers and x as labeled (i.e., a parameter for the amphiphilicity of the dendrimers; see Sec. 3.2.1) at packing fraction $\phi_m = 0.248$ and temperature $k_B T = 1.4 \varepsilon_{CC}^{D7}$. The color scale is shown at the right-hand side of the diagrams. The black isolines indicate where the pair distribution function $g(r, \alpha)$ attains 90% of the height of the nearest-neighbor peak. (r, α) -values with less than 10 realizations are superposed by diagonal lines colored in white.

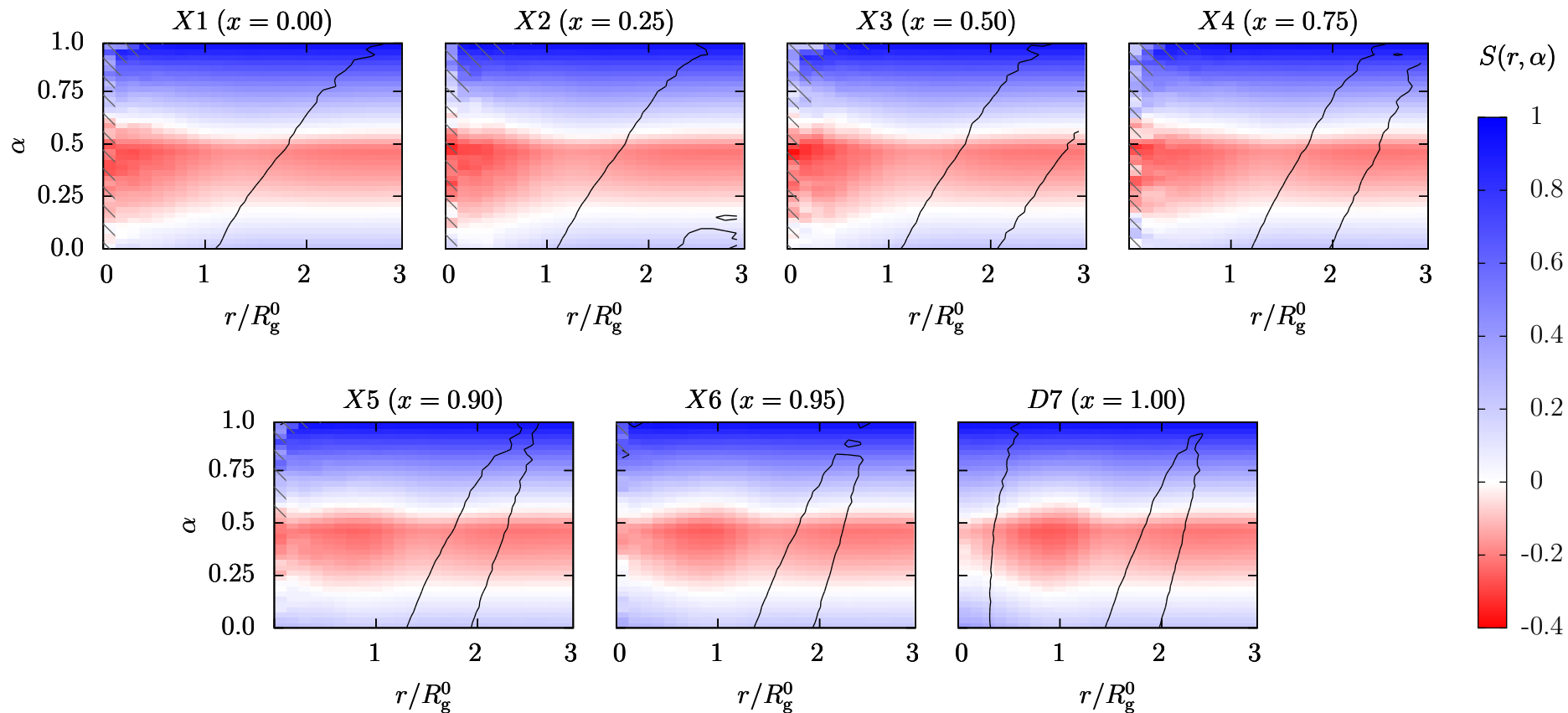


Figure 6.22.: Contour plots of the orientational order parameter $S(r, \alpha)$ for G4 dendrimers and x as labeled (i.e., a parameter for the amphiphilicity of the dendrimers; see Sec. 3.2.1) at packing fraction $\phi_m = 0.248$ and temperature $k_B T = 1.4 \varepsilon_{CC}^{D7}$. The color scale is shown at the right-hand side of the diagrams. The black isolines indicate where the pair distribution function $g(r, \alpha)$ attains 90% of the height of the nearest-neighbor peak. (r, α) -values with less than 10 realizations are superposed by diagonal lines colored in gray.

7. Conclusions

In this work we have studied the shape as well as the spatial and orientational equilibrium configurations of amphiphilic dendrimers in a bulk liquid via molecular dynamics simulations in the canonical ensemble. To be more specific, we computed the radius of gyration tensor for each dendrimer in the ensemble and used its eigenvalues and eigenvectors to quantify the shape of the dendrimers and their relative orientation with respect to other molecules. We used the radius of gyration as a measure of size of the dendrimers and quantified its shape by the asphericity b , the acylindricity c , the relative shape anisotropy δ as well as the normalized volume $V_{\text{ell}}/V_{\text{sphere}}$. Moreover, we studied the relative orientation of pairs of dendrimers in terms of the α parameter and the orientational correlation function S (see Sec. 5.2.2 for their definitions). Here, α quantifies the orientation of both long axes of two interacting dendrimers relative to the center-to-center vector while S is a measure for the mutual orientation of their long axes. Our investigations included different values of generation numbers of the dendrimer, the influence of the temperature as well as of the packing fraction and the changes in the properties when tuning the amphiphilic behavior.

We started by investigating the shape of so-called D7-type dendrimers with varying generation number G ranging from $G = 2$ up to $G = 8$ at a packing fraction $\phi_m = 0.248$ and temperature $k_B T = 1.4 \varepsilon_{\text{CC}}^{\text{D7}}$. In all cases, we used a system size of 220 dendrimers with 3080 monomers in the case of $G = 2$ and 224840 in the case of $G = 8$. We showed that the size of the dendrimers (in terms of the radius of gyration) increases monotonically with G . We also found that dendrimers are in general prolate. However, they become increasingly spherical at higher generations; their asphericity b , acylindricity c as well as the relative shape anisotropy δ decrease with increasing G while their normalized volume $V_{\text{ell}}/V_{\text{sphere}}$ is approaching unity (except for G6 as discussed thoroughly in Sec. 6.1).

We then focused on D7-type G4 dendrimers and studied their shape as well as their spatial and orientational order at various temperatures ranging from $k_B T = 0.7 \varepsilon_{\text{CC}}^{\text{D7}}$ up to $k_B T = 1.8 \varepsilon_{\text{CC}}^{\text{D7}}$, considering three different packing fractions $\phi_m = 0.248$, $\phi_m = 0.153$ and $\phi_m = 0.095$. Again, we used a system size of 220 dendrimers with a total amount of 13640 monomers. Our results for the shape of the dendrimers indicate a pronounced trend towards bigger and more prolate molecules with increasing temperature. Concerning the relative orientation of two neighboring dendrimers our most important finding is, that the existence of an antinematic [66] liquid phase (illustration shown in Fig. 7.1) as indicated by a mixture of end-to-end --- , parallel || and perpendicular || , ⊥ and ⊥ configurations [22], strongly depends on the temperature as well as on the packing fraction; this special arrangement is also highly correlated to the presents of full particle overlaps. To be more specific, this antinematic liquid phase was found for intermediate temperatures at a packing fraction $\phi_m = 0.248$, for low temperatures in the case of $\phi_m = 0.153$ and for the lowest temperature at a packing fraction $\phi_m = 0.095$. In all the other cases, parallel

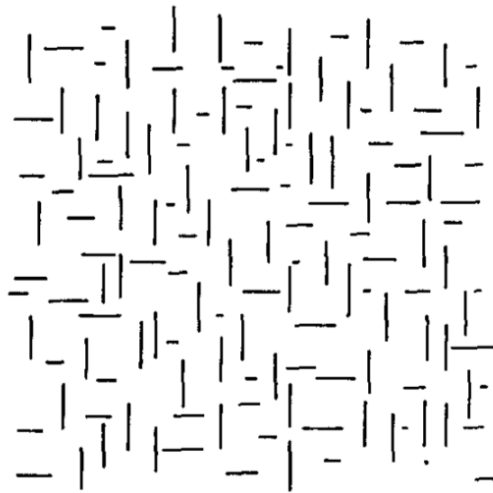


Figure 7.1.: Illustration of the antinematic phase. From: K. Sokalski and T. Ruijgrok [66].

configurations \parallel of nearest neighbors are preferred, suggesting a nematic [19], rather than an antinematic liquid phase. Georgiou et al. demonstrated that the antinematic arrangement is consistent with the A15 crystal lattice [16, 22] (shown in Fig. 7.2) as found in experiments [18] and suggested that its stability [19] may be related to the elongated shape and deformability of dendrimers. A possible arrangement of dendrimers in the A15 lattice is shown in Fig. 7.3.

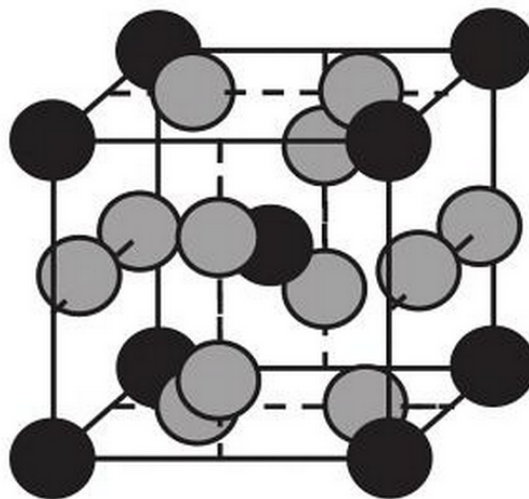


Figure 7.2.: Unit cell of the A15 lattice. The columnar sites are colored in gray whereas the interstitial sites are colored in black. From: W. Kung [67]

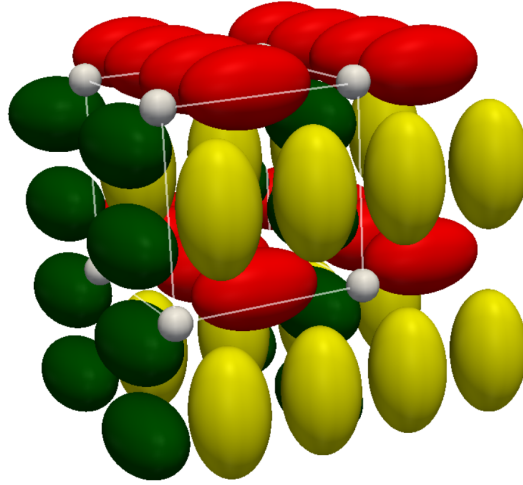


Figure 7.3.: The A15 lattice decorated by ellipsoids; the dodecahedral interstitial sites (small white spheres shown for clarity) lack a preferred orientation. The different colors indicate the different types of columnar site pairs. This arrangement captures the antinematic nature as observed in dendrimer liquids. From: I. Georgiou [16]

Finally, we investigated how shape as well as spatial and orientational properties change while reducing the amphiphilicity of the dendrimers from D7-type to X1-type at a packing fraction $\phi_m = 0.248$ and temperature $k_B T = 1.4 \varepsilon_{CC}^{D7}$. Again, we used a system size of 220 G4 dendrimers with a total amount of 13640 monomers. With this change in amphiphilicity the size of the dendrimers became bigger due to the linear increase of the bond length between shell and core monomers; the molecules also tended towards less spherical shapes. In addition, the system underwent a transition from a bulk liquid with a mixture of end-to-end --- , parallel || , and perpendicular I^\bullet , L and L^\bullet configurations with distinct amount of clustering to a liquid where nearest neighbors prefer || configurations and where full particle overlaps are very rare. The decreasing difference between shell and core particles leads, hence, to a nematic rather than antinematic phase, as already discussed above for the case of high temperatures and low packing fractions.

In summary, decreasing amphiphilicity as well as increasing temperature leads to a bigger and more prolate shape of the dendrimers. This temperature dependence of the shape is more pronounced at lower packing fractions. Furthermore, the dendrimer liquid shows a high amount of full particle overlap at low temperatures and high packing fractions. The amphiphilic character of the dendrimers is thereby essential for this formation of clusters. The presence of particle overlaps, on the other hand, is fundamental for the antinematic arrangement. Georgiou et al. [16, 22] concluded, that the antinematic packing pattern is a strong indicator for the A15 lattice, however, we recommend to further analyze this link.

Appendices

A. Interaction parameters

In this appendix we present the exact values for the interaction parameters of X1- to X6-type dendrimers as introduced in Sec. 3.2.1.

X1 (x = 0.00)

FENE	$K_{\mu\nu}(d_{CC}^{D7})^2$	$l_{\mu\nu}^0/d_{CC}^{D7}$	$R_{\mu\nu}/d_{CC}^{D7}$
CC	20	2.8125	0.5625
CS	20	2.8125	0.5625
Morse	$\varepsilon_{\mu\nu}$	$\alpha_{\mu\nu}d_{CC}^{D7}$	$d_{\mu\nu}/d_{CC}^{D7}$
CC	0.014	19.2	1.50
CS	0.014	19.2	1.50
SS	0.014	19.2	1.50

Table A.1.: Interaction parameters of the potentials Eq. (3.4) and Eq. (3.5) for X1-type dendrimers

X2 (x = 0.25)

FENE	$K_{\mu\nu}(d_{CC}^{D7})^2$	$l_{\mu\nu}^0/d_{CC}^{D7}$	$R_{\mu\nu}/d_{CC}^{D7}$
CC	25	2.57813	0.515626
CS	20	2.8125	0.5625
Morse	$\varepsilon_{\mu\nu}$	$\alpha_{\mu\nu}d_{CC}^{D7}$	$d_{\mu\nu}/d_{CC}^{D7}$
CC	0.189	16.0	1.375
CS	0.014	19.2	1.4375
SS	0.014	19.2	1.50

Table A.2.: Interaction parameters of the potentials Eq. (3.4) and Eq. (3.5) for X2-type dendrimers

X3 (x = 0.50)

FENE	$K_{\mu\nu}(d_{CC}^{D7})^2$	$l_{\mu\nu}^0/d_{CC}^{D7}$	$R_{\mu\nu}/d_{CC}^{D7}$
CC	30	2.34375	0.46875
CS	20	2.8125	0.5625
Morse	$\varepsilon_{\mu\nu}$	$\alpha_{\mu\nu}d_{CC}^{D7}$	$d_{\mu\nu}/d_{CC}^{D7}$
CC	0.365	12.8	1.25
CS	0.014	19.2	1.375
SS	0.014	19.2	1.50

Table A.3.: Interaction parameters of the potentials Eq. (3.4) and Eq. (3.5) for X3-type dendrimers

X4 (x = 0.75)

FENE	$K_{\mu\nu}(d_{CC}^{D7})^2$	$l_{\mu\nu}^0/d_{CC}^{D7}$	$R_{\mu\nu}/d_{CC}^{D7}$
CC	35	2.10938	0.421875
CS	20	2.8125	0.5625
Morse	$\varepsilon_{\mu\nu}$	$\alpha_{\mu\nu}d_{CC}^{D7}$	$d_{\mu\nu}/d_{CC}^{D7}$
CC	0.539	9.6	1.125
CS	0.014	19.2	1.3125
SS	0.014	19.2	1.50

Table A.4.: Interaction parameters of the potentials Eq. (3.4) and Eq. (3.5) for X4-type dendrimers

X5 (x = 0.90)

FENE	$K_{\mu\nu}(d_{CC}^{D7})^2$	$l_{\mu\nu}^0/d_{CC}^{D7}$	$R_{\mu\nu}/d_{CC}^{D7}$
CC	38	1.96875	0.360
CS	20	2.8125	0.5625
Morse	$\varepsilon_{\mu\nu}$	$\alpha_{\mu\nu}d_{CC}^{D7}$	$d_{\mu\nu}/d_{CC}^{D7}$
CC	0.644	7.68	1.05
CS	0.014	19.2	1.275
SS	0.014	19.2	1.50

Table A.5.: Interaction parameters of the potentials Eq. (3.4) and Eq. (3.5) for X5-type dendrimers

X6 (x = 0.95)

FENE	$K_{\mu\nu}(d_{CC}^{D7})^2$	$l_{\mu\nu}^0/d_{CC}^{D7}$	$R_{\mu\nu}/d_{CC}^{D7}$
CC	39	1.921875	0.3675
CS	20	2.8125	0.5625
Morse	$\varepsilon_{\mu\nu}$	$\alpha_{\mu\nu}d_{CC}^{D7}$	$d_{\mu\nu}/d_{CC}^{D7}$
CC	0.679	7.04	1.025
CS	0.014	19.2	1.2625
SS	0.014	19.2	1.50

Table A.6.: Interaction parameters of the potentials Eq. (3.4) and Eq. (3.5) for X6-type dendrimers

B. Random distribution of α -parameter

For the sake of completeness, we provide in this appendix the code for calculating the random distribution of the parameter α from Ref. [16] and as referred to in Sec. 5.3. The distribution is shown in Fig. B.1.

```
#!/usr/bin/python
import sys
import numpy as np
import numpy.random as ran
import math as m

steps = 5000000

def ran_theta():
    return m.acos(ran.uniform(-1.0,1.0))
def ran_phi():
    return ran.uniform(0.0,2*m.pi)

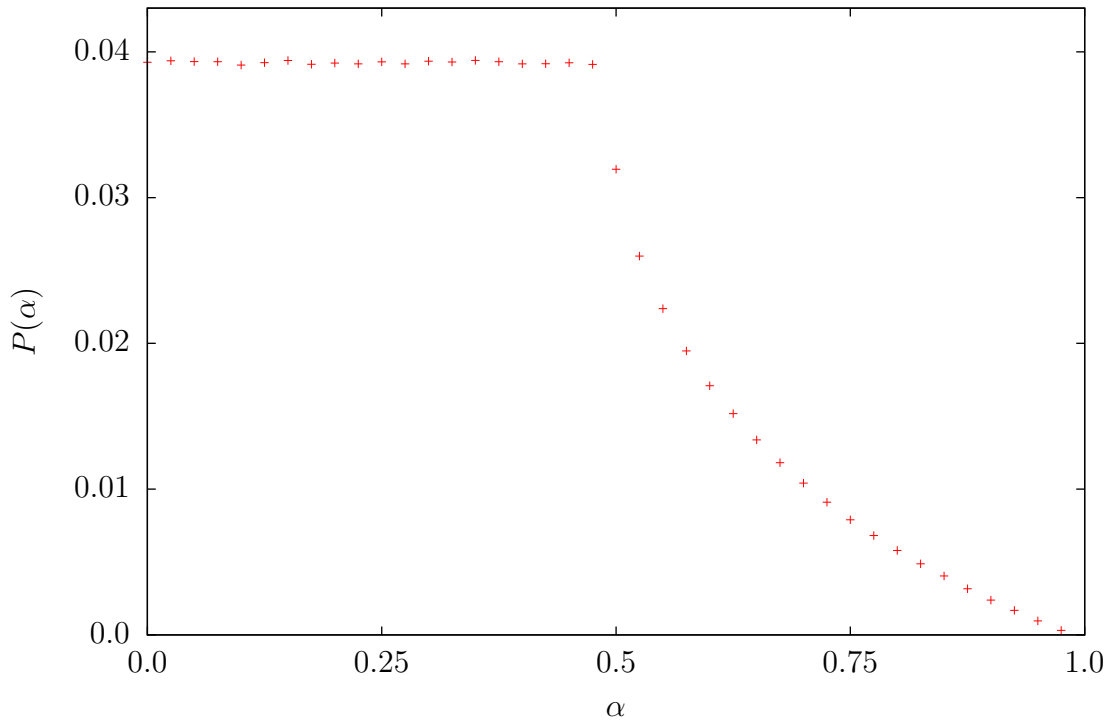
R = []
L1 = []
L2 = []
Alpha = []
count = 0

for s in range(steps):
    if s%100000 == 0:
        print "step=",s,"/",steps
        th1 = ran_theta()
        th2 = ran_theta()
        thr = ran_theta()
        ph1 = ran_phi()
        ph2 = ran_phi()
        phr = ran_phi()
    # Create three random unit vectors
    # l1: long axes first molecule
    # l2: long axes second molecule
    # r: center to center vector
```

```

l1 = (m.sin(th1)*m.cos(ph1),m.sin(th1)*m.sin(ph1),m.cos(th1))
l2 = (m.sin(th2)*m.cos(ph2),m.sin(th2)*m.sin(ph2),m.cos(th2))
r = (m.sin(thr)*m.cos(phr),m.sin(thr)*m.sin(phr),m.cos(thr))
L1.append(l1)
L2.append(l2)
R.append(r)
# Calculate alpha parameter
alpha = (np.dot(l1,r))**2+(np.dot(l2,r))**2
Alpha.append(alpha)
# Create histograms of alpha
H_alpha, bin_alpha = np.histogram(Alpha,bins=40,range=[0,2.0])
# output to files
fz_new = open("alpha_dist_40bins.out","w")
for i in range(len(H_alpha)):
    fznew.write("%4d\t%13.6f\t%13.6f\t%13.6f\n"
    %(i,bin_alpha[i]/2.0,H_alpha[i]/float(steps),H_alpha[i]))

```

Figure B.1.: Random distribution of α

Bibliography

- [1] M. Doi, *Soft matter physics* (Oxford University Press, 2013).
- [2] C. N. Likos, *Effective interactions in soft condensed matter physics*, Physics Reports **348**, 267 (2001).
- [3] C. Kittel, *Introduction to solid state physics* (John Wiley and Sons, Inc, 2005).
- [4] R. Jones, *Soft condensed matter* (Oxford University Press, 2002).
- [5] F. Vögtle, N. Werner and G. Richardt, *Dendrimer chemistry* (Wiley, 2009).
- [6] E. Buhleier, W. Wehner and F. Vögtle, *Cascade- and nonskid-chain-like syntheses of molecular cavity topologies*, Synthesis, 155 (1978).
- [7] D. A. Tomalia, A. M. Naylor and W. A. Goddard, *Starburst dendrimers: molecular-level control of size, shape, surface chemistry, topology, and flexibility from atoms to macroscopic matter*, Angewandte Chemie International Edition **29**, 138 (1990).
- [8] T. J. Prosa, B. J. Bauer, E. J. Amis, D. A. Tomalia and R. Scherrenberg, *A saxs study of the internal structure of dendritic polymer systems*, Journal of Polymer Science Part B: Polymer Physics **35**, 2913 (1997).
- [9] A. Topp, B. J. Bauer, D. A. Tomalia and E. J. Amis, *Effect of solvent quality on the molecular dimensions of pamam dendrimers*, Macromolecules **32**, 7232 (1999).
- [10] I. O. Götze and C. N. Likos, *Microscopic and coarse-grained correlation functions of concentrated dendrimer solutions*, Journal of Physics: Condensed Matter **17**, 1777 (2005).
- [11] S. Huißmann, C. N. Likos and R. Blaak, *Conformations of high-generation dendritic polyelectrolytes*, Journal of Materials Chemistry **20**, 10486 (2010).
- [12] B. M. Mladek, G. Kahl and C. N. Likos, *Computer assembly of cluster-forming amphiphilic dendrimers*, Physical Review Letters **100**, 028301 (2008).
- [13] B. M. Mladek and D. Frenkel, *Pair interactions between complex mesoscopic particles from widom's particle-insertion method*, Soft Matter **7**, 1450 (2011).
- [14] M. Ballauff and C. N. Likos, *Dendrimers in solution: insight from theory and simulation*, Angewandte Chemie International Edition **43**, 2998 (2004).
- [15] P. K. Maiti, G. Wang and W. A. Goddard, *Structure of pamam dendrimers: generations 1 through 11*, Macromolecules **37**, 6236 (2004).
- [16] I. A. Georgiou, *Simulations of soft matter systems*, PhD thesis (Technische Universität Wien, 2014).

- [17] V. S. K. Balagurusamy, G. Ungar, V. Percec and G. Johansson, *Rational design of the first spherical supramolecular dendrimers self-organized in a novel thermotropic cubic liquid-crystalline phase and the determination of their shape by x-ray analysis*, Journal of the American Chemical Society **119**, 1539 (1997).
- [18] X. Zeng, G. Ungar, Y. Liu, V. Percec, A. E. Dulcey and J. K. Hobbs, *Supramolecular dendritic liquid quasicrystals*, Nature **428**, 157 (2004).
- [19] Y. Li, S.-T. Lin and W. A. Goddard, *Efficiency of various lattices from hard ball to soft ball: theoretical study of thermodynamic properties of dendrimer liquid crystal from atomistic simulation*, Journal of the American Chemical Society **126**, 1872 (2004).
- [20] S. Prestipino and F. Saija, *Phase diagram of gaussian-core nematics*, The Journal of Chemical Physics **126**, 194902 (2007).
- [21] A. Nikoubashman and C. N. Likos, *Self-assembled structures of gaussian nematic particles*, Journal of Physics: condensed matter **22**, 104107 (2010).
- [22] I. A. Georgiou, P. Ziherl and G. Kahl, *Antinematic local order in dendrimer liquids*, Europhysics Letters **106**, 44004 (2014).
- [23] B. M. Mladek, D. Gottwald, G. Kahl, M. Neumann and C. N. Likos, *Formation of polymorphic cluster phases for a class of models of purely repulsive soft spheres*, Physical Review Letters **96**, 045701 (2006).
- [24] B. M. Mladek, *Exotic phenomena in the phase behaviour of soft matter systems*, PhD thesis (Technische Universität Wien, 2007).
- [25] M. P. Allen and D. J. Tildesley, *Computer simulation of liquids*, eng, Oxford science publications (Clarendon Pr., Oxford, 1987), XIX, 385 S.
- [26] J. Rudnick and G. Gaspari, *The aspheryity of random walks*, Journal of Physics A: Mathematical and General **19**, L191 (1986).
- [27] D. Chandler, *Introduction to modern statistical mechanics* (Oxford University Press, 1987).
- [28] D. Greenwood, *Classical dynamics* (Dover Publications, 1997).
- [29] M. Rubinstein and R. H. Colby, *Polymer physics* (Oxford University Press, 2003).
- [30] B. Helms and E. W. Meijer, *Dendrimers at work*, Science **313**, 929 (2006).
- [31] G. M. Dykes, *Dendrimers: a review of their appeal and applications*, Journal of Chemical Technology and Biotechnology **76**, 903 (2001).
- [32] Y. Cheng and D. Tomalia, *Dendrimer-based drug delivery systems: from theory to practice* (Wiley, 2012).
- [33] R. Esfand and D. A. Tomalia, *Poly(amidoamine) (pamam) dendrimers: from biomimicry to drug delivery and biomedical applications*, Drug Discovery Today **6**, 427 (2001).
- [34] C. C. Lee, J. A. MacKay, J. M. J. Frechet and F. C. Szoka, *Designing dendrimers for biological applications*, Nature Biotechnology **23**, 1517 (2005).
- [35] F. Aulenta, W. Hayes and S. Rannard, *Dendrimers: a new class of nanoscopic containers and delivery devices*, European Polymer Journal **39**, 1741 (2003).

- [36] A. E. Beezer, A. S. H. King, I. K. Martin, J. C. Mitchel, L. J. Twyman and C. F. Wain, *Dendrimers as potential drug carriers; encapsulation of acidic hydrophobes within water soluble pamam derivatives*, Tetrahedron **59**, 3873 (2003).
- [37] F. Zhao and W. Li, *Dendrimer/inorganic nanomaterial composites: tailoring preparation, properties, functions, and applications of inorganic nanomaterials with dendritic architectures*, Science China Chemistry **54**, 286 (2011).
- [38] D. A. Tomalia, H. Baker, J. Dewald, M. Hall, G. Kallos, S. Martin, J. Roeck, J. Ryder and P. Smith, *Dendritic macromolecules: synthesis of starburst dendrimers*, Macromolecules **19**, 2466 (1986).
- [39] P. de Gennes and H. Herve, *Statistics of "starburst" polymers*, Journal de Physique Lettres **44**, 351 (1983).
- [40] R. L. Lescanec and M. Muthukumar, *Configurational characteristics and scaling behavior of starburst molecules: a computational study*, Macromolecules **23**, 2280 (1990).
- [41] D. Boris and M. Rubinstein, *A self-consistent mean field model of a starburst dendrimer: dense core vs dense shell*, Macromolecules **29**, 7251 (1996).
- [42] M. Murat and G. S. Grest, *Molecular dynamics study of dendrimer molecules in solvents of varying quality*, Macromolecules **29**, 1278 (1996).
- [43] P. Welch and M. Muthukumar, *Tuning the density profile of dendritic polyelectrolytes*, Macromolecules **31**, 5892 (1998).
- [44] J. K. Young, G. R. Baker, G. R. Newkome, K. F. Morris and C. S. Johnson, *"Smart" cascade polymers. modular syntheses of four-directional dendritic macromolecules with acidic, neutral, or basic terminal groups and the effect of ph changes on their hydrodynamic radii*, Macromolecules **27**, 3464 (1994).
- [45] C. N. Likos, A. Lang, M. Watzlawek and H. Löwen, *Criterion for determining clustering versus reentrant melting behavior for bounded interaction potentials*, Physical Review E **63**, 031206 (2001).
- [46] R. B. Bird, *Dynamics of polymeric liquids* (Wiley, 1977).
- [47] P. M. Morse, *Diatomic molecules according to the wave mechanics. ii. vibrational levels*, Physical Review **34**, 57 (1929).
- [48] D. Landau and K. Binder, *A guide to monte carlo simulations in statistical physics* (Cambridge University Press, 2000).
- [49] L. Verlet, *Computer experiments on classical fluids. i. thermodynamical properties of lennard-jones molecules*, Phys. Rev. **159**, 98 (1967).
- [50] W. C. Swope, H. C. Andersen, P. H. Berens and K. R. Wilson, *A computer simulation method for the calculation of equilibrium constants for the formation of physical clusters of molecules: application to small water clusters*, The Journal of Chemical Physics **76**, 637 (1982).
- [51] M. Borm and T. von Karman, *Periodic boundary conditions*, Physikalische Zeitschrift **13**, 297 (1912).

- [52] S. Nosé, *A unified formulation of the constant temperature molecular dynamics methods*, The Journal of Chemical Physics **81**, 511 (1984).
- [53] G. Newkome, C. Moorefield and F. Vögtle, *Dendritic molecules: concepts, syntheses, perspectives* (Wiley, 2008).
- [54] S. Hadizadeh, A. Linhananta and S. S. Plotkin, *Improved measures for the shape of a disordered polymer to test a mean-field theory of collapse*, Macromolecules **44**, 6182 (2011).
- [55] R. P. Smith and E. M. Mortensen, *Bond and molecular polarizability tensors. i. mathematical treatment of bond tensor additivity*, The Journal of Chemical Physics **32**, 502 (1960).
- [56] A. K. Soper, *Orientational correlation function for molecular liquids: the case of liquid water*, The Journal of Chemical Physics **101**, 6888 (1994).
- [57] C. Gray and K. Gubbins, *Theory of molecular fluids: i: fundamentals* (Oxford University Press, 1984).
- [58] G. Arfken, H. Weber and F. Harris, *Mathematical methods for physicists: a comprehensive guide* (Elsevier, 2012).
- [59] U. Gedde, *Polymer physics* (Springer, 1995).
- [60] S. Fakirov, *Oriented polymer materials* (Wiley, 2008).
- [61] N. Platé and S. Schnur, *Liquid-crystal polymers* (Plenum Press, 1993).
- [62] D. C. Rapaport, *The art of molecular dynamics simulation* (Cambridge university press, 2004).
- [63] J. M. Haile, *Molecular dynamics simulation: elementary methods* (Wiley, 1997).
- [64] S. Plimpton, *Fast parallel algorithms for short-range molecular dynamics*, J Comp Phys **117**, 1 (1995).
- [65] D. A. Lenz, R. Blaak and C. N. Likos, *Adsorption characteristics of amphiphilic dendrimers*, Soft Matter **5**, 2905 (2009).
- [66] K. Sokalski and T. Ruijgrok, *An anti-nematic phase of liquid crystals*, Physica A: Statistical Mechanics and its Applications **126**, 280 (1984).
- [67] W. Kung, *Geometry and phase transitions in colloids and polymers* (World Scientific, 2009).

Acknowledgements

Gerhard Kahl, für Ihre Unterstützung, Ihre Freundlichkeit und das interessante Thema dieser Arbeit.

Marta, for your help and support throughout this work and for your patience in answering my numerous questions.

Meinen Freunden, für die zahlreichen Ablenkungen vom oft entbehrungsreichen Studium.

Meinen Eltern, für eure Liebe, eure bedingungslose Unterstützung und den finanziellen Rückhalt.

Lilly, für deine Aufmunterungen, deine Liebe und die wunderbare Zeit mit dir.

Facts

In the course of this thesis 318 GB of data (e.g., restart files, log files, output of center of mass and gyration tensor) were produced by the molecular dynamics simulations program LAMMPS¹ within a computation time of 1.883.708 core-hours on VSC-2². This time was approximately needed for (information from LAMMPS log files):

- communication due to parallel computing $\sim 42\%$
- computation of monomer-monomer interactions $\sim 35\%$
- computation of bonding interactions $\sim 2\%$
- building and rebuilding the neighbour list $\sim 0.5\%$
- data output $\sim 0.08\%$
- everything else $\sim 21\%$

¹<http://lammps.sandia.gov/> (online 11.12.2014)

²<http://vsc.ac.at/> (online 11.12.2014)

How did it get so late so soon?
Dr. Seuss